Searching For Radio Emission From Magnetars

Patrick Lazarus
Department of Physics
McGill University
Montréal, Québec
Canada

A Thesis submitted to the
Faculty of Graduate Studies and Research
in partial fulfillment of the requirements for the degree of
Master of Science

This is dedicated to the late, great Five-Hole Sam.

Contents

List of Figures

List of Tables

Abstract

Observations of five magnetars and two magnetar candidates carried out at 1950 MHz with the Green Bank Telescope in 2006-2007 were searched for periodic emission and bright single pulses. Also, Target-of-Opportunity observations of magnetar 4U 0142+61 at increasing intervals following its 2006 X-ray bursts were obtained. No radio emission was detected. The non-detections were used to place luminosity upper limits of $\lesssim 4$ mJy kpc^2 for periodic emission and $\lesssim 10$ Jy kpc^2 for single pulse emission. These are the most stringent limits yet for the magnetars observed. The implication of the non-detections and their resulting luminosity upper limits together with previous results is discussed, as is the importance of further radio observations of radio-loud and radio-quiet magnetars.

Résumé

Des observations radio de cinq magnétars et deux candidats magnétar effectuée à 1950 MHz avec le télescope de Green Bank en 2006-2007 ont été analyse dans le but de détecter des émissions périodiques et des impulsions radios isolées. En outre, des observations "Target-of-Opportunity" du magnétar 4U 0142+61, effectuées à intervalles croissants, suite à ses sursauts X en 2006, ont été obtenues. Aucune émission radio n'a été détecté. Les non-détections ont été utilisées pour placer des limites supérieures de luminosité de $\lesssim 4$ mJy kpc^2 pour les émissions périodiques et de $\lesssim 10$ Jy kpc^2 pour les impulsions isolées. Ce sont les limites les plus strictes obtenues jusqu'à maintenant pour les magnétars observées. Nous discutons les implications des non-détections et leurs limites supérieures de luminosité comparées aux résultats précédents, de même que l'importance des observations radios supplémentaires de magnétars silencieux ou bruyant dans les ondes radios.

Acknowledgments

First and foremost, I thank my family for their never-ending questions about how my thesis is progressing. Because of you I've wanted nothing more than to finish my thesis as soon as possible. Mostly to stop the interrogation. Thank you for the extra motivation.

I also thank my supervisor, Vicky, for providing me (and the rest of the McGill Pulsar Group) with the evironment and tools to do world-class research, and for sharing her expertise.

My thesis wouldn't be what it is if it weren't for the help of Maggie, Seb and Slavko, whose combined efforts have likely found more typos in the following document than there are words. Thnaks.

I acknowledge David Champion for being the PI on the telescope proposal that eventually became my Master's thesis. David, along with Jason Hessels, are responsible for performing the observations for the project. Without them I would have no data. Thanks, but where's the rest of it?

Rim Dib and Fernando Camilo have graciously provided me with unpublished information that has been useful in data analysis and the interpretation of results.

I thank Scott Ransom for writing `PRESTO`, which I have used to analyse the data in this project, and for providing technical support. Speaking of technical support, thanks to Paul Mercure for fixing the Borg everytime I break it.

Finally, I acknowledge the financial support of NSERC CGS-M and PGS-M extension awards, as well as a Trottier "Accelerator" Fellowship from McGill University, they keep my apartment warm in winter and put food on the table, even if it's only ramen.

Preface

Statement of Originality and Contribution of Authors

It is our intention to submit the work presented in this thesis, in a modified format, for publication in the Astrophysical Journal. Co-authors of the eventual article are: Dr. David Champion, Dr. Rim Dib, Dr. Jason Hessels, and Prof. Victoria Kaspi.

The contributions of the co-authors are as follows: David Champion was the principal investigator on the telescope project that acquired the data analysed here. David Champion and Jason Hessels performed the observations. Rim Dib provided up-to-date ephemrides of 1E1841−045, 1E 2259+586, and 4U 0142+61. Victoria Kaspi provided guidance on the project, data analysis and interpretation of results.

1 Introduction

Go forward

Move ahead

Try to detect it

It's not too late

Whip It

Devo

1.1 Neutron Stars and Pulsars

When $\gtrsim 9M_\odot$[1] stars reach the end of the main sequence, they can no longer support their own weight (e.g. Carroll & Ostlie, 2006). When this occurs the core of the star implodes and its outer layers are ejected. The resulting explosion is called a *supernova*. Neutron stars, supported by neutron degeneracy pressure, are the remnants of the supernova explosions of massive stars ($9M_\odot$ – $25M_\odot$). For even more massive progenitor stars ($\gtrsim 25M_\odot$), neutron degeneracy pressure is no longer sufficient to support the compact remnant, and thus it is believed that the explosions of these extremely massive stars will produce black holes. Less massive main sequence stars ($\lesssim 9M_\odot$) do not undergo supernova explosions. Rather, they become white dwarfs.

This thesis will focus on a particular class of neutron star, pulsars, and various sub-classes of pulsars. Black holes and white dwarfs will not be considered.

Pulsars are highly magnetized, rapidly rotating neutron stars. Observed spin periods[2] of pulsars range from 1.4 ms to 11.8 s. Pulsars are also observed to be spinning down. That is, their spin periods are observed to increase with time. The

[1] Where $1M_\odot = 1.98892 \times 10^{30}$ kg is the mass of the Sun.

[2] See the ATNF Pulsar Catalogue: http://www.atnf.csiro.au/research/pulsar/psrcat/ (Manchester et al., 2005).

mechanism by which this slowing occurs is assumed to be dominated by magnetic dipole braking. This assumption leads to the simplified model for a pulsar: a rotating neutron star with a dipolar magnetic field (see Figure 1.1).

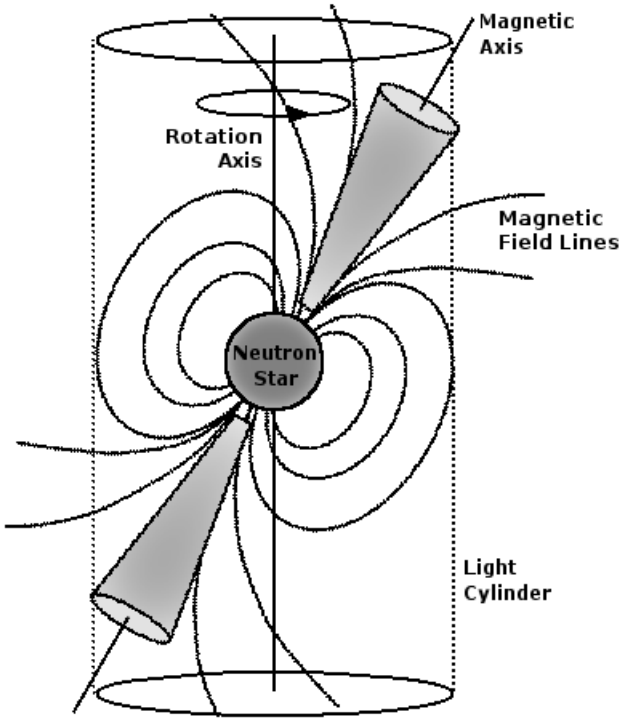

Figure 1.1: Simple model of a pulsar: a rotating neutron star with a dipolar magnetic field misaligned with the rotation axis of the star. Figure modified from Lorimer & Kramer (2004).

With a few basic assumptions, it is possible to use the above simple model to estimate various parameters, such as the pulsar's spin-down luminosity, $\dot{E}$, the magnetic field strength at the pulsar's surface, B, and the characteristic age of the pulsar, τ. The following discussion will outline of how each of these parameters is estimated (for additional details see, e.g., Lorimer & Kramer, 2004).

The spin-down luminosity, typically measured in erg s^{-1}, is the amount of energy released by the pulsar per unit time due to the slowing of its rotation. It is simply the time derivative of the rotational energy of the pulsar,

$$\dot{E} = \frac{d}{dt}\left(\frac{1}{2}I\Omega^2\right) = -I\Omega\dot{\Omega}, \tag{1.1}$$

where I is the moment of inertia of the neutron star[1] and Ω is its rotational angular frequency. When written in terms of the pulsar's spin period, $P = 2\pi/\Omega$, and factoring out all numerical constants, Equation 1.1 becomes

$$\dot{E} \simeq 4 \times 10^{31} \text{erg s}^{-1} \left(\frac{\dot{P}}{10^{-15}} \right) \left(\frac{P}{\text{s}} \right)^{-3}. \tag{1.2}$$

By equating Equation 1.1 with the power radiated by a rotating magnetic dipole (e.g. Griffiths, 1999) it is possible to infer the magnetic field strength at the surface of the pulsar,

$$B = \sqrt{\frac{3c^3}{8\pi^2} \frac{I}{R^6 \sin^2 \alpha} P\dot{P}}, \tag{1.3}$$

where α is the misalignment angle between the magnetic and rotation axes. By assuming an orthogonal rotator, $\alpha = 90°$, a semi-quantitative expression relating the period and spin-down rate to the star's magnetic field strength can be derived,

$$B \simeq 10^{12} \text{G} \left(\frac{\dot{P}}{10^{-15}} \right)^{1/2} \left(\frac{P}{\text{s}} \right)^{1/2}. \tag{1.4}$$

The magnetic field strengths calculated using Equations 1.3 or 1.4 are not measurements. Considering all the assumptions required, the inferred magnetic field strengths should only be considered as order-of-magnitude estimates.

When the spin-down luminosity is equated to the power radiated by a rotating magnetic dipole, the relation in terms of frequency (as opposed to angular frequency), $\nu = \Omega/2\pi$, can be written in terms of a power law,

$$\dot{\nu} = -K\nu^n, \tag{1.5}$$

where K is a constant related to I, R and α, and n is the *braking index*. For the specific case described above, magnetic dipole braking in a vacuum, the braking index[2] is $n = 3$. Integrating Equation 1.5 gives an expression for the age of the pulsar. The

[1] The value $I = 10^{45}$ g cm^2 is typically used for the moment of inertia, assuming a uniform sphere with radius, $R = 10$ km, and mass, $M = 1.4 M_\odot$.

[2] Braking indices are measured to be in the range $1.4 \leq n \leq 2.91$ (Livingstone et al., 2006).

characteristic age of the pulsar is obtained by making some simplifying assumptions: the braking index is $n = 3$ and the spin period of the pulsar at birth is much less than its current spin period. The characteristic age of a pulsar, in terms of P and $\dot{P}$, is given by

$$\tau = \frac{P}{2\dot{P}} \simeq 16 \text{ Myr} \left(\frac{P}{\text{s}}\right) \left(\frac{\dot{P}}{10^{-15}}\right)^{-1} . \tag{1.6}$$

A common way of reviewing the main properties of a pulsar (i.e. spin period, spin-down rate, spin-down luminosity, magnetic field strength and characteristic age), and comparing them with those of other known pulsars is to use the period-period derivative diagram (P-$\dot{P}$ diagram, see Figure 1.2). At least three regions of the P-$\dot{P}$ diagram can be identified: the rapidly rotating, low-B pulsars in the bottom left of the diagram are the millisecond pulsars, which will not be discussed in this thesis. The central region of the diagram contains the bulk of the pulsar population, which will be introduced in Section 1.2. The pulsars located in top-right region of the plot are the slowly rotating, high-B magnetars, which will be discussed in Section 1.3.

1.2 Rotation-Powered Pulsars

Nearly all of the 1880 pulsars listed in the ATNF Pulsar Catalogue are rotation powered (Manchester et al., 2005). As the name suggests, the energy source that produces the observed emission of rotation-powered pulsars comes from the star's rotation. The rotational energy of the star is converted and released as electromagnetic radiation.

Most rotation-powered pulsars emit radio waves, and most were first detected at radio frequencies, however the radio emission takes up only a small fraction of the pulsar's energy budget, typically one part in 10^5 of $\dot{E}$ (Ghosh, 2007). Radio spectra are typically fit with power laws, $S_\nu \propto \nu^\alpha$. The average radio pulsar spectral index is $\langle\alpha\rangle = -1.8 \pm 0.2$ (Maron et al., 2000). In addition to being observed at radio frequencies, rotation-powered pulsars have also been observed (and even discovered) by their X-ray and γ-ray emission (for reviews see Kaspi et al., 2006; Abdo et al.,

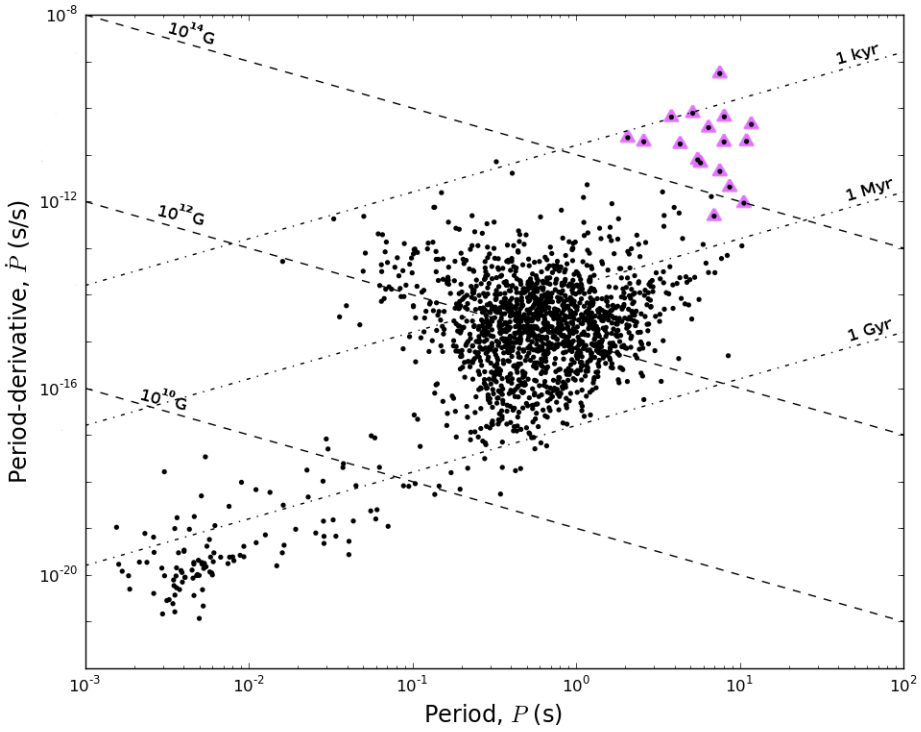

Figure 1.2: The period-period derivative diagram. Each point represents a known pulsar. The points in the top right of the plot, highlighted with triangles, are the *magnetars*: highly magnetized, slowly rotating pulsars. Lines of constant magnetic field strength (dashed) and constant characteristic age (dash-dotted) are also shown.

2010, respectively)[1].

1.3 Magnetically Powered Pulsars: Magnetars

The term "magnetar" was first used by Duncan & Thompson (1992) to describe highly magnetized neutron stars ($B \sim 10^{14}$ to 10^{15} G). Magnetars fall into two sub-classes, the Soft Gamma Repeaters (SGRs) and the Anomalous X-Ray Pulsars (AXPs). Duncan & Thompson (1992) outline the birth conditions required to produce magnetar-strength fields via dynamos.

According to the "McGill SGR/AXP Online Catalog" maintained by the McGill

[1]A small number of pulsars have also been observed to pulse at optical wavelengths (see Shearer & Golden, 2002, and references therein).

Pulsar Group[1], there are currently 16 confirmed magnetars, 7 SGRs and 9 AXPs, as well as 3 magnetar candidates (2 SGRs and 1 AXP candidate), as of July 2010. In addition to listing both confirmed and candidate magnetars, the catalog also provides an overview of the observational properties of each magnetar.

Historically, SGRs and AXPs were considered different classes of object. SGRs were identified by hard X-ray and soft γ-ray bursts, whereas AXPs were discovered by anomalously bright persistent X-ray pulsations (Woods & Thompson, 2006). Recently the division between SGRs and AXPs has been blurred. SGR-like bursts have been detected from AXPs (for a review, see Kaspi, 2007), and persistent X-ray pulsations have been observed from SGRs (Kouveliotou et al., 1998).

In contrast with rotation-powered pulsars, magnetars are very variable objects; they have a wide variety of X-ray emission behaviour such as: short (~ 100 ms) bursts, outbursts containing many short bursts, giant flares lasting hundreds of seconds that exhibit pulsations in their fading tails[2], flux enhancements lasting hundreds of days and X-ray pulse profile variations (see Woods & Thompson, 2006; Kaspi, 2007, for more details). Magnetars also have complicated timing properties such as: timing noise, torque variations, and glitches[3] (again, see Woods & Thompson, 2006; Kaspi, 2007, for more details). Magnetars typically have more X-ray luminosity than can be explained by their spin-down luminosity (i.e. $L_X > \dot{E}$). Finally, recent observations indicate that radio emission from magnetars has characteristic properties that are not shared with rotation-powered pulsars. These properties will be outlined below, in Section 1.4.

1.4 Transition Objects

It was theorized that pulsars with very strong magnetic fields, $B \gtrsim 4 \times 10^{13}$ G, could not produce radio emission (Baring & Harding, 1998). However, pulsars with magnetic field strengths surpassing the limit derived by Baring & Harding (1998) were

[1] http://www.physics.mcgill.ca/~pulsar/magnetar/main.html

[2] Giant flares have only been observed in 3 SGRs and never in an AXP (Woods & Thompson, 2006).

[3] Glitches are sudden events in which the spin frequency of the magnetar increases.

eventually discovered (Camilo et al., 2000; McLaughlin et al., 2003), suggesting that radio emission from magnetars is a possibility. The belief that because both magnetars and rotation-powered pulsars are neutron stars it is reasonable to expect them to have similar observational properties, or even for there to be a continuum of possible behaviours, with transition objects existing and showing properties intermediate between the two populations was given credence by the discovery of high-B radio pulsars.

It was not until 2006 that there was a firm detection of pulsed radio emission from a magnetar[1] (Woods & Thompson, 2006; Camilo et al., 2006). Still, most magnetars observed at radio frequencies have not been detected (this work; Burgay et al., 2006; Crawford et al., 2007). However, an increasing number of sources exhibit behaviour commonly associated with rotation-powered pulsars, as well as produce magnetar-like emission. The observational properties of four pulsars known to straddle the divide, XTE J1810−197, 1E 1547.0−5408, PSR J1622−4950, and PSR J1846−0258, will now be described. The general properties of these transition objects are outlined in Table 1.1. Three of the four transition objects have been detected at radio frequencies. They have been found to have common properties that are not shared with the bulk of the rotation-powered pulsar population. In particular, there is the trifecta of radio variability: variable spectral index, variable pulse profiles, and variable flux density. The range of specral indices observed from radio-detected magnetars (including variations in their spectrum) are very flat (or rising), which is in contrast to the majority of rotation-powered pulsars.

Understanding how and why these transition objects demonstrate both magnetar and rotation-powered emission properties will hopefully offer insight into the pulsar emission mechanism and the nature of matter in ultra-strong magnetic fields. To this end, the ultimate goal of this thesis is to discover more transition objects.

Due Diligence

Before discussing specific transition objects, a few quick notes are required.

[1]See the discussion about marginal, unconfirmed radio detections below.

First, there have been reports of detections of magnetars (SGR 1900+14 and 1E 2259+586) at 111 MHz using the Pushchino Radio Astronomy Observatory in Russia (Shitov et al., 2000; Malofeev et al., 2005). Due to the transit design of the telescope, observations were were limited to a ~ 5 minutes of integration time; the detections were marginal[1] and have not been confirmed using another telescope (e.g. Lorimer & Xilouris, 2000). Because of the lack of confirmation, these results, while they may be the first detections of pulsed radio emission from magnetars, will not be discussed further.

Also, following giant flares by SGR 1900+14 and SGR 1806−20, in each case, decaying radio emission was detected (Frail et al., 1999; Gaensler et al., 2005). In both cases the emission was unpulsed and was proposed to be relativistic particles ejected during the flare. In contrast, the focus of this thesis is to detect *pulsed* emission from magnetars.

XTE J1810−197

The AXP XTE J1810−197 was discovered in mid-2003 following an X-ray flux enhancement that occured in late 2002 or early 2003 (Ibrahim et al., 2004). Persistent X-ray pulsations were detected with a period of $P = 5.54$ s. See Table 1.1 for a listing of properties of XTE J1810−197. Ibrahim et al. (2004) suggested XTE J1810−197 is a magnetar based on the X-ray pulsations detected, the strength of the implied magnetic field and its soft AXP-like X-ray spectrum (below 10 keV).

Approximately one year after XTE J1810−197 was discovered, it was detected in the radio band, at 1400 MHz, by Halpern et al. (2005) in data from the Very Large Array (VLA) taken as part of the Multi-Array Galactic Plane Imaging Survey (MAGPIS). A point source[2] was detected at the position of the AXP with a flux density of 4.5 ± 0.5 mJy.

Pulsed radio emission was detected from XTE J1810−197 on March 17, 2006, at

[1]The significance of the detections reported in Shitov et al. (2000) and Malofeev et al. (2005) are not reported and the pulse profiles prsented are not convincing.

[2]The VLA was in B configuration, and the full width at half-maximum of the beam was $6''$.

1400 MHz, using the Parkes telescope (Camilo et al., 2006). Multi-frequency follow-up observations have found that XTE J1810−197 has an unusual radio spectrum. The spectral index is observed to vary in the range $0 \leq \alpha \leq -1.0$, where α is defined in Section 1.2 (Camilo et al., 2007c). Even though α is observed to vary, it is consistently flatter (i.e. closer to 0) than the average value of $\langle\alpha\rangle = -1.8 \pm 0.2$ for rotation-powered pulsars (Maron et al., 2000). The flux density, S_ν, of XTE J1810−197 is also variable, changing by factors of ∼2 on day time scales (Camilo et al., 2006) and fading on a time scale of $\sim$ 1 – 2 years (Camilo et al., 2007a). Finally, the pulse profile of XTE J1810−197 is also observed to vary (Camilo et al., 2007a).

1E 1547.0−5408

The discovery of 1E 1547.0−5408 as a magnetar (with radio emission) followed a different path than that of XTE J1810−197. First, 1E 1547.0−5408, a previously known, but unclassified source of X-rays, was proposed to be a magnetar by Gelfand & Gaensler (2007). This identification was based on the X-ray source's spectrum, as well as its coincidence with an infrared source, and a radio shell proposed to be a supernova remnant (Gelfand & Gaensler, 2007). In mid-2007, radio pulsations from 1E 1547.0−5408 were detected using the Parkes radio telescope (Camilo et al., 2007b). Subsequently, X-ray pulsations were detected (Halpern et al., 2008). The measured spin-down luminosity, $\dot{E} = 1.0 \times 10^{35}$ erg s^{-1}, is comparable to the X-ray luminosity reported by Halpern et al. (2008), $L_X = 1.7 \times 10^{35} (d/9 \text{ kpc})^2$ erg s^{-1}, supporting the prediction by Gelfand & Gaensler (2007) that 1E 1547.0−5408 is a magnetar. Since then, X-ray outbursts were observed in late 2008 and again in early 2009[1] (see Ng et al., 2010, and references therein). Table 1.1 contains radio, X-ray and spin properties of 1E 1547.0−5408.

PSR J1622−4950

In April 2009, PSR J1622−4950, a radio pulsar with a period of $P = 4.326$ s was discovered in the High Time Resolution Universe survey being conducted with the

[1]See *Swift* GCNs 8311 and 8833: http://gcn.gsfc.nasa.gov/gcn3_archive.html.

Parkes radio telescope (Levin et al., 2010). The radio properties of this pulsar are strikingly similar to those of the two confirmed radio-loud magnetars discussed above (see Table 1.1). These similarities, and a coincident faint X-ray source, lead Levin et al. (2010) to conclude that PSR J1622−4950 is a radio-loud magnetar in X-ray quiescence.

PSR J1846−0258

The young 326-ms pulsar, PSR J1846−0258, in the supernova remnant Kes 75, is a radio-quiet X-ray pulsar with a relatively large inferred magnetic field strength, $B = 4.9 \times 10^{13}$ G (Gotthelf et al., 2000). Mid-2006 observations of PSR J1846−0258 detected five magnetar-like X-ray bursts and an X-ray flux enhancement (Gavriil et al., 2008; Ng et al., 2008; Kumar & Safi-Harb, 2008). These bursts are the first recorded magnetar-like emission from a seemingly rotation-powered pulsar. The detection of bursts and associated flux enhancement reinforce the interpretation that there is a continuum of magnetar-like behaviour whose manifestation is related to the strength of the object's magnetic field (Gavriil et al., 2008). Following the detection of bursts from PSR J1846−0258, a search for radio emission, both for bright single pulses and for periodic signals, was conducted (Archibald et al., 2008). No radio pulsations were detected. Also, no bright single pulses from PSR J1846−0258 were detected.

1.5 Searches For Radio Emission From Other Magnetars

The discoveries of radio-loud high-magnetic-field pulsars and magnetars have spurred on observations of other magnetars in the hopes of detecting radio emission (Burgay et al., 2006; Crawford et al., 2007). Falling short of this goal, the observations are still useful for placing stringent upper limits on any radio emission, which will be useful if one turns on in the radio band.

No detections of radio emission from magnetars other than the ones discussed in Section 1.4 have been published. However, limits of $S_{1400} \lesssim 20$ μJy have been placed on three Southern magnetars, 1RXS J170849.0−400910, 1E 1841−045 and

1E 1048.1−5937, and one magnetar candidate, AX J1845−0258 (Crawford et al., 2007)[1]. Also, upper limits on the flux density of single pulses at 1400 MHz from the above-listed four sources have been placed in the range 0.9 – 1.1 Jy (Crawford et al., 2007).

In this thesis, data on five magnetars and two magnetar candidates, including one magnetar and one magnetar candidate searched by Crawford et al. (2007), are searched for periodic emission and bright single pulses using the Green Bank Telescope.

1.6 Layout of this Thesis

The layout of the rest of this thesis is as follows. Chapter 2 describes the entire data path for this project, from acquiring data at the telescope, through the data analysis, to a description of the data products. Chapter 3 reports the details of the observations searched. The results of the analysis performed on these data are presented in Chapter 4. Chapter 5 discusses these results and provides their context within the body of previous work on the subject. Finally, Chapter 6 concludes this thesis.

[1]Similar limits for the same four objects were achived by Burgay et al. (2006). However, the limits published by Crawford et al. (2007) are more stringent.

Table 1.1: Spin, X-ray and radio properties of magnetar / high-B radio pulsar transition sources.

	XTE J1810−197	**1E 1547.0−5408**	**PSR J1622−4950**	**PSR J1846−0258**
		Spin and Derived Properties		
Spin period, P (s)	5.54	2.07	4.33	0.326
Spin-down rate, $\dot{P}$ (10^{-11} s s^{-1})	1.8	2.3	1.7	0.7
Magnetic field strength, B (10^{14} G)	3	2	3	0.5
Spin-down luminosity, $\dot{E}$ (10^{33} erg s^{-1})	4	100	8.5	8100
Characteristic age, τ (yr)	5000	1400	4000	884
Distance, d (kpc)	∼10	∼9	∼9	∼6
		X-ray Properties		
X-ray Luminosity[a], L_X (10^{33} erg s^{-1})	1600 (0.5 – 9 keV)	170 (1 – 8 keV)	2.5 (0.3 – 10 keV)	41 (3 – 10 keV)
		Radio Properties		
Dispersion Measure, DM (cm^{-3} pc)	180	830	820	–[b]
Radio Profile FWHM (%)	2.7 (at 1400 MHz)	12 (at 2300 MHz)	∼11 (at 3100 MHz)	–[b]
Luminosity at 1400 MHz[ac], L_{1400} (mJy kpc^2)	65	320	400	–[b]
Spectral index, α ($S_\nu \propto \nu^\alpha$)	$-1.0 \leq \alpha \leq 0$	–[d]	> 0	–[b]

Notes:

[a] Luminosities calculated using distance reported here.

[b] No radio emission is detected from PSR J1846−0258 (Archibald et al., 2008).

[c] Values reported are typical. Sources are observed to be variable within a factor of a few.

[d] The radio spectrum of 1E 1547.0−5408 cannot be described by a single spectral index.

References: *XTE J1810−197*: Ibrahim et al. (2004), Camilo et al. (2006), Camilo et al. (2007c); *1E 1547.0−5408*: Camilo et al. (2007b), Camilo et al. (2008), Halpern et al. (2008); *PSR J1622−4950*: Levin et al. (2010); *PSR J1846−0258*: Gavriil et al. (2008), Livingstone et al. (2006), Leahy & Tian (2008)

2
The Data Path and Data Products

The new No. 2: We want information...

No. 6: You won't get it!

The new No. 2: By hook or by crook, we will.

The Prisoner

Patrick McGoohan

and George Markstein

In this chapter the data path is outlined, tracing each of the relevant steps: the collection/detection of radio waves and how radio signals are recorded as data files (Section 2.1), the removal of radio frequency interference and data analysis (Section 2.2), a description of the end-products that are viewed by eye (Section 2.3), and finally, an end-to-end example provides some details and summarizes the chapter (Section 2.4).

2.1 Recording Data

All data analysed in this thesis were acquired using the 100 m Robert C. Byrd Green Bank radio Telescope (GBT). The GBT is operated by the National Radio Astronomy Observatory[1] and is located in Green Bank, West Virginia. The GBT's primary reflector, a 100 by 110 m parabolic segment of a larger hypothetical structure, is unobstructed by its off-axis feed[2]. The GBT is the largest fully-steerable single-dish telescope ever constructed. Observations were carried out at S-band ($\sim$ 1950 MHz). The GBT's S-band receiver is a cooled, single feed, dual linear polarisation

[1] http://www.nrao.edu

[2] See GBT website: http://www.gb.nrao.edu/gbt/.

receiver covering the band 1680 - 2650 MHz[1]. Data were recorded using the GBT Pulsar Spigot backend, an autocorrelation spectrometer (Kaplan et al., 2005). A spectrometer is required for radio observations of pulsars, to correct for dispersion caused by the interstellar medium (see Section 2.2.2).

Autocorrelation spectrometers are flexible receiver back-ends that allow for various bandwidths, frequency resolutions and sample times. Autocorrelation spectrometers take advantage of the fact that the autocorrelation function and power spectrum make up a Fourier Transform pair[2] (e.g. Wilson et al., 2009). This type of spectrometer operates by delaying the input signal (voltage as a function of time), multiplying it with the original signal, summing, and recording the result. The result is a *lagged product*, where lag refers to the time delay. Many lagged products are computed by re-delaying the signal and repeating the multiply/sum steps. The larger the number of lagged products output, the greater the frequency resolution will be when the Fourier Transform of the lagged products is computed (Lorimer & Kramer, 2004). The step of recording lagged products is repeated in every time sample. The Fourier Transforms to convert lagged products to a power spectrum are generally computed subsequent to an observing session.

The GBT Pulsar Spigot has many modes provided by its design (Kaplan et al., 2005). However, for the purposes of this project, data were recorded with a central frequency of 1850 MHz and a total bandwidth of 800 MHz divided into 1024 channels, sampled every 81.92 μs. The data are converted from lags to observing frequency spectra. In this process the bottom 200 MHz of the band is removed, resulting in a central frequency of 1950 MHz, a total bandwidth of 600 MHz and 768 channels. The sample time is unchanged. The bottom portion of the observing band is removed because the GBT S-band receiver has no sensitivity below $\sim$ 1650 MHz.

The GBT Pulsar Spigot has a data rate of 23.8 MB s^{-1}. A total of 24.1 hours of observations were performed, resulting in $\sim$ 20 TB of raw data. These data were

[1]See the GBT proposer's guide: http://www.gb.nrao.edu/gbtprops/man/GBTpg.pdf.

[2]For additional details of Fourier Transforms, autocorrelations, power spectra, etc. see Bracewell (2000).

transfered to external hard drives and shipped to McGill University for analysis.

2.2 Data Analysis: General Techniques

The data analysis employed to search for radio pulsations from magnetars is composed of five steps: excising radio frequency interference (RFI), dedispersion, searching for periodic signals using a Fast Fourier Transform (FFT), folding the data, and searching for bright individual pulses, commonly known as *single pulses*. To perform all five steps, programs from `PRESTO`[1], a suite of pulsar search software by Ransom (2001), were used. Each of these steps will now be described in detail.

2.2.1 Excising Radio Frequency Interference

Terrestial RFI introduces spurious signals into the data that make it difficult, or in some cases impossible, to find genuine pulsar signals. It is vital that RFI is properly removed from all observations in order to maximize sensitivity to pulsars. Using `PRESTO`'s `rfifind` program, RFI instances are removed by breaking each frequency channel into blocks. The duration of the blocks used is defined by the user. The mean, median and standard deviation of each block are computed. Statistics are also computed for the Fourier Transform of each block. Blocks whose mean or standard deviation is different by more than a user-defined threshold when compared to their entire time interval or channel are flagged to be masked. Masked blocks are replaced with the mean data value for the given channel, excluding the 10% smallest values and the 10% largest values. This will remove the deleterious effect of the interference without greatly affecting the statistics of the data. Also, blocks whose maximum power spectrum value is larger than another user-defined threshold when compared to their entire time interval or channel are also flagged to be masked.

RFI is highly variable and difficult to automatically identify and remove from data. For this reason, each RFI mask is reviewed by eye to check for individual channels and time sub-integrations with an unacceptably large fraction of data masked. The

[1] http://www.cv.nrao.edu/∼sransom/presto/

mask may be modified to ensure each of these offending channels and sub-integrations are masked entirely.

2.2.2 Dedispersion

Radio waves passing through the interstellar medium (ISM) are delayed due to free electrons along the line-of-sight. The amount of delay incurred depends on the integrated column density of free electrons along the path, as well as the frequency of the signal. The dispersion relation is (Lorimer & Kramer, 2004),

$$t = \mathcal{D} \times \frac{\mathrm{DM}}{f^2}, \tag{2.1}$$

where t is the time delay in seconds, DM is the dispersion measure,

$$\mathrm{DM} = \int_0^d n_e \mathrm{d}l, \tag{2.2}$$

a path integral over electron number density, n_e, along the line-of-sight, d is the distance to the pulsar, and $\mathcal{D}$ is a constant,

$$\mathcal{D} = \frac{e^2}{2\pi m_e c}. \tag{2.3}$$

In pulsar astronomy DM is typically measured in cm^{-3} pc.

Pulsars are broadband radio sources (e.g. Lorimer & Kramer, 2004). The dispersion of a pulsar signal will cause a once narrow pulse to be smeared out as different frequencies reach the telescope at slightly different times. This phenomenon can easily cause pulsars to be undetectable. For example, the smearing across a 600 MHz band centred at 1950 MHz is ~ 70.5 ms, for DM = 100 cm^{-3} pc. This means pulsars with $P \lesssim 70.5$ ms will not be detectable without first correcting for dispersion. Pulsars with longer periods may still be detected in uncorrected data, but their signal-to-noise ratio will be reduced relative to the detection using corrected data. In order to maximize sensitivity to a pulsar, the frequency band is divided evenly into many individual channels. Each channel is then shifted according to the delay given by Equation 2.1. This will correct for dispersive smearing across the observing band (see

Figure 2.1 for an example). Unfortunately, since channels of finite width are used, there will still be some smearing within each channel which cannot be removed by this technique. If the 600 MHz band, from the example above, is divided evenly into 768 channels, the amount of smearing that cannot be removed is only ~ 144 μs at the low-end of the observing band, where dispersion has a larger effect.

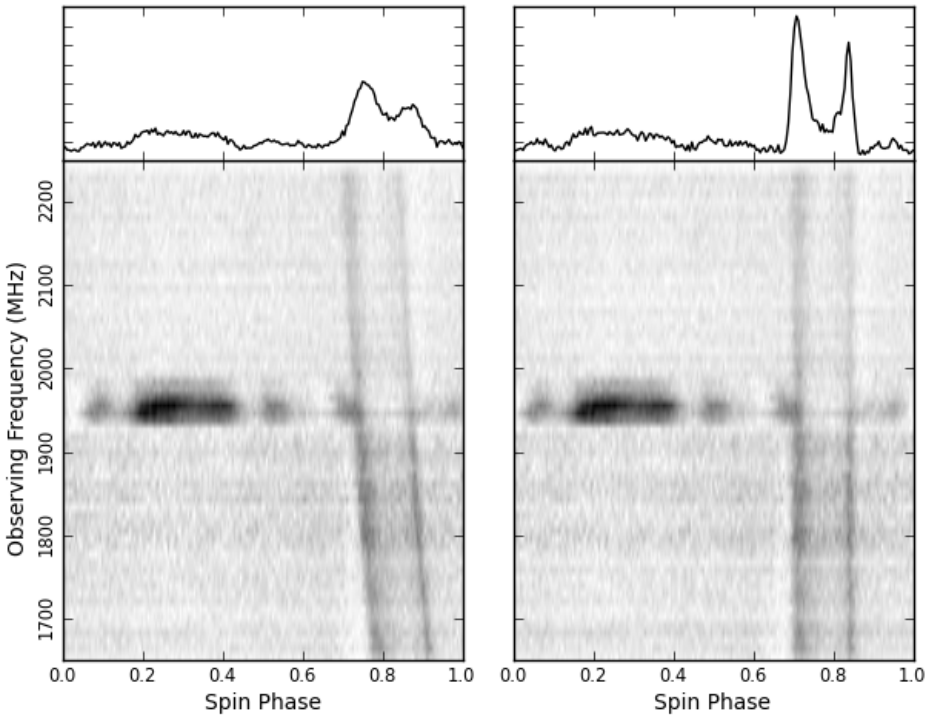

Figure 2.1: *Left*: A GBT Spigot S-band observation of PSR B1839−04 (P=1.84 s, DM=196 cm^{-3} pc) without being corrected for dispersion. The greyscale represents signal intensity, increasing from white to black. *Right*: The same observation after dedispersion. Notice the increased signal-to-noise ratio and sharper features in the dedispersed pulse profile (top panels). The darker horizontal structure is narrowband RFI.

When searching for radio emission, the DM is not known *a priori*, thus many trial values must be used to maintain sensitivity to a large range of DMs. A *dedispersion plan* defines how widely to space trial DM values in order to ensure a desired time resolution and minimize the amount of computation required. This plan is defined as follows. The spacing of trial DM values is chosen such that a pulsar signal with a DM that falls between two adjacent trials will be smeared across the entire observing bandwidth by no more than the desired resolution. Also, to reduce computation

time, the dedispersion plan dictates at what values of DM data can be reduced in size by adding adjacent samples. This is known as *downsampling*. The DMs at which downsampling occurs are where the smearing in a single channel is comparable to the sample time. Downsampling also has the effect of reducing the total number of samples in a data file, making it less time consuming to analyse. DM step sizes are re-computed for each downsampled time resolution.

At this stage, RFI masks are applied, removing RFI instances identified by the technique described in Section 2.2.1. Also, the dedispersed time series are *barycentred*, which accounts for the position and motion of the Earth by modifying the data to be as if they had been recorded at the centre of mass (or barycentre) of the Solar system[1].

For the purposes of this thesis, dedispersion plans were designed using `PRESTO`'s `DDplan.py` and dedispersed time series were created using `PRESTO`'s `prepsubband`.

2.2.3 Searching for Periodic Signals

For each dedispersed time series, a search for periodic signals is performed. First, the real Fourier Transform (i.e. one-sided FT) of the time series is computed. By searching the resulting power spectrum for significant peaks, it is possible to identify sinusoidal signals in the time series. However, most radio pulsars have non-sinusoidal pulse profiles[2]. Typical duty cycles for radio pulsars range from $\delta = W/P \simeq 2.5\%$ to 5.5%, where P is the spin period and W is the width of the pulse (e.g. Lyne & Smith, 2005), although some pulsars have larger duty cycles (for example, see Figure 2.1). Harmonic summing is used to improve sensitivity to narrow pulse profiles. The number of significant harmonics is inversely related to the pulsar's duty cycle (e.g. Lorimer & Kramer, 2004).

[1] Barycentering is also important for pulsar timing. Additional details can be found in Lorimer & Kramer (2004).

[2] Individual pulses are variable and typically too faint to detect. However, the signal-to-noise ratio of a coherent sum of 100s or 1000s of pulses, an *integrated pulse profile*, is improved by a factor $\sim \sqrt{N}$, where N is the number of pulses summed. In most cases, integrated pulse profiles are extremely stable (e.g. Lorimer & Kramer, 2004). More details are presented in Section 2.2.4.

The search of each Fourier Transform was done using `PRESTO`'s `accelsearch` program. The range of frequencies searched was ~ 0.1 Hz to ~ 1000 Hz[1]. `accelsearch` searches through the Fourier components by defining the position of the highest harmonic. The lower-frequency harmonics are positioned accordingly. Lower harmonics that do not fall on integer frequency bins sustain a loss of sensitivity. To regain lost sensitivity, *interbinning* is used to estimate the value of the Fourier Transform at a fractional bin number using the values of the two neighbouring integer bins. All peaks in the harmonically summed power spectrum surpassing a user-defined significance threshold are stored in a list of candidates. These candidates are optimized in a second pass through the Fourier Transform. In this optimization step, a more careful interpolation technique is used to identify the most significant frequency of the highest harmonics and more accurately estimate the value of the Fourier components at fractional bin positions.

As the name suggests, `accelsearch` is used to search for accelerated pulsars. Pulsars in binary systems exhibit acceleration along the line of sight resulting in Doppler shifts (Lorimer & Kramer, 2004). These Doppler shifts cause once-narrow peaks in the power spectrum to be variably offset from their true frequency and for their power to be spread over neighbouring bins over the course of an observation. `accelsearch` uses a frequency domain finite impulse response match filtering technique to regain sensitivity to binary pulsars (Ransom et al., 2002). Since none of the known magnetars is in a binary system[2], no acceleration searches were performed on the data in this thesis.

The above procedure for finding periodicity candidates is applied independently to each dedispersed time series. The lists of candidates are combined to determine if the same periodicities are found at multiple neighbouring trial DMs, which is expected for genuine signals, and the optimal DM is determined. Harmonically related candidates are discarded in favour of the candidate at the fundamental frequency, as

[1] All known magnetars have frequencies in the 0.1 Hz to 1 Hz range. The additional frequency range searched here is to maintain sensitivity to any other pulsars in the field-of-view.

[2] See the McGill Pulsar Group's magnetar catalog.

are candidates with DM < 2 cm^{-3} pc, to reduce the chance of reporting interference signals. This process is called *sifting*. The end-result of sifting is an aggregate list of periodicity candidates sorted by significance.

2.2.4 Folding

For most pulsars, individual pulses are not bright enough to be detected above the noise present in the data[1] (e.g. Lorimer & Kramer, 2004). For this reason, the data must be *folded*, a process illustrated in Figure 2.2.

Folding, simply put, involves slicing a time series into chunks of data, each of which has a duration equal to the pulsar's spin period, or the period of a search candidate. These slices of data are then summed together. Since pulsars are so regular, the signal present in the data will add coherently ($O(N)$, where N is the number of pulses summed), whereas the noise will add incoherently ($O\left(\sqrt{N}\right)$.)

In this thesis, time series data were folded using `PRESTO`'s `prepfold`. An example of `prepfold`'s output is described in Section 2.3. Data were folded in two situations. First, data were folded using the periods of candidates indentified in periodicity searching. In this case, the only time series folded is the one dedispersed at the DM where the candidate is found to be most significant. Second, if the observation is of a magnetar with an available *ephemeris*[2], for example, by being observed at another waveband (typically X-ray), then all dedispersed time series were folded using the known period at the epoch of the observation, as predicted by the ephemeris.

2.2.5 Searching for Single Pulses

The last step in searching for radio emission is to search for bright single pulses. As mentioned in Section 2.2.4, individual pulses from most pulsars are not bright enough to be detected above the noise. However, some pulsars emit pulses that are individ-

[1] This is not always the case. A technique designed to search for bright individual pulses will be presented in Section 2.2.5.

[2] An ephemeris is a set of astrometric and spin parameters that can be used to predict the period and phase of a pulsar.

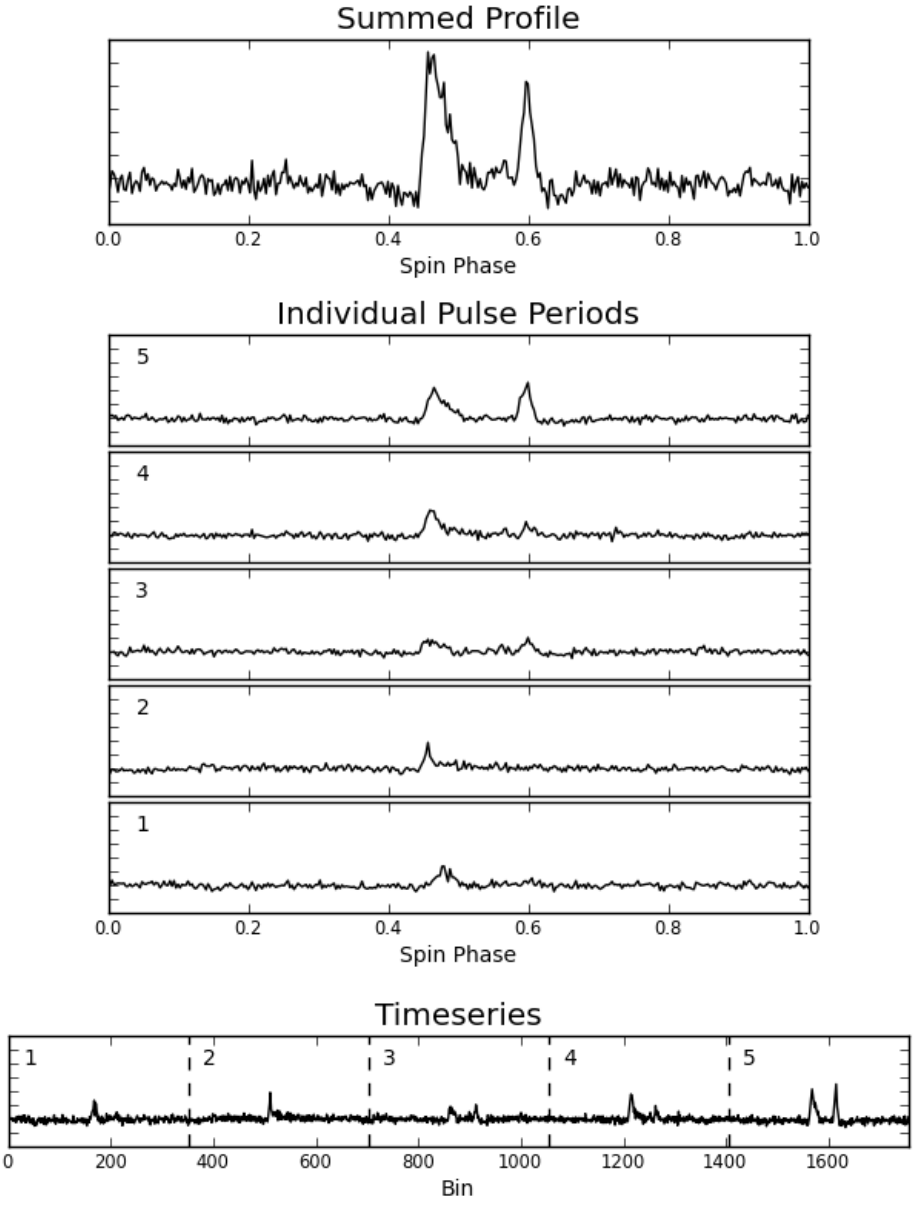

Figure 2.2: *Bottom*: A time series is sliced into segments each of duration equal to the pulse period. *Middle*: The individual pulses are lined up and summed. *Top*: The resulting summed profile has a higher signal-to-noise ratio than the individual pulses. The data in this figure are from a GBT Spigot S-band observation of PSR B1839−04 (P=1.84 s, DM=196 cm^{-3} pc). Here the individual pulses are sufficiently bright to be visible without summing, however this is not generally the case.

ually detectable. A match filtering technique is used by `single_pulse_search.py`, which is part of `PRESTO`, to search for these bright pulses.

A single pulse is most significant when the effective sample time[1] is equal to the duration of the pulse (Cordes & McLaughlin, 2003). To increase sensitivity to pulses longer than the intrinsic sampling time, the dedispersed time series are convolved with top-hat filters of various widths. The smoothed time series are then searched for peaks larger than a user-defined threshold. The time, significance, and width of all identified pulses are recorded. Less significant pulses found to be overlapping with, or sufficiently close to, more significant pulses are discarded in favour of the latter. The matched filtering search algorithm is run on all dedispersed time series generated for an observation. Diagnostic plots are produced using all single pulse candidates from all dedispersed time series. An example of the diagnostic plots used is described in Section 2.3.

To determine the veracity of a single pulse, the time of arrival of the signal as a function of time and frequency is examined to confirm that it adheres to the dispersion relation (see Equation 2.1 and Figure 2.3). Pulses that do not follow the expected relation are considered non-astrophysical and are discarded.

2.3 Data Products

Both algorithms used to search for emission from pulsar data (Fourier Transforms and folding, and matched filtering of bright pulses) produce diagnostic plots that must be interpreted by eye to determine if they represent true detections. In this section, examples of the two types of plots will be shown and their main features will be outlined.

For every periodicity candidate, the time series dedispersed with the DM that maximizes the signal is folded using `prepfold`. The plot produced by `prepfold` is the main diagnostic used for periodicity candidates. An example of this type of plot for PSR B1839−04 is shown in Figure 2.4. The figure consists of four parts (starting in

[1]The effective sample time includes contributions from dispersion, scattering and instrumental effects.

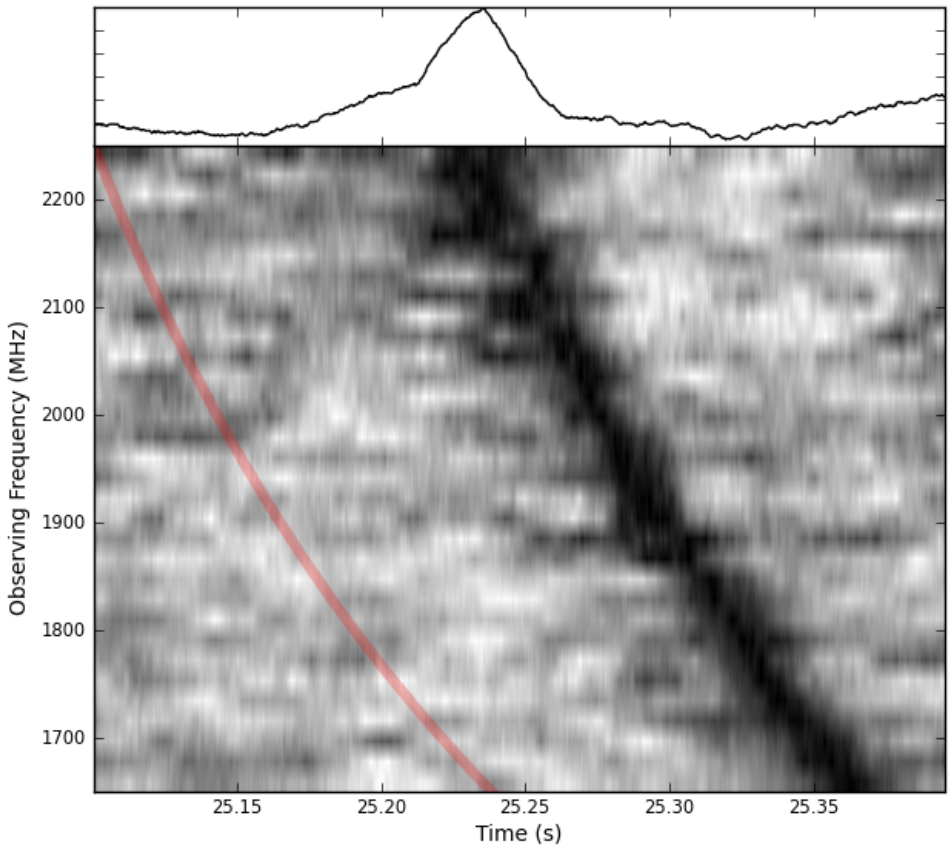

Figure 2.3: Plot of signal intensity as a function of frequency and sample number of a single pulse from PSR B1839−04, used to verify the pulse's astrophysical nature. The red trace is the frequency vs. time relation for a DM of 196 cm^{-3} pc. The top subplot shows the dedispersed signal as a function of time. Each data sample is 327.68 μs. The data are smoothed by a top hat 70 samples wide.

the top-left, progressing clockwise): the integrated pulse profile; textual information describing the data and fold parameters; a colour χ^2 map from the optimization of P and $\dot{P}$ used to fold[1]. The χ^2 values come from comparing the resulting profile with a constant. The optimized P and $\dot{P}$ values used for folding are indicated by the black point, and the two satellite plots are slices of the plot along the horizontal and vertical directions through the (P, $\dot{P}$) pair used. Finally, the last plot is a greyscale of the sub-integrations, where each row is an integrated pulse profile of a subset of the entire observation. This helps determine if the emission is persistent, and if the period is constant throughout the observation. The plot to the right of the sub-integrations is the χ^2 values comparing the cumulative profile integrated thus far to a constant.

The other diagnostic plot used to identify pulsar emission is based on the single pulse search and is produced by `single_pulse_search.py`. An example of a single pulse plot from an observation of PSR B1839−04 is shown in Figure 2.5. At the top of the single pulse plot is information about the observation. The middle row of plots consists of (from left to right): a histogram of the number of single pulses found as a function of signal-to-noise ratio; a histogram of the number of single pulses as a function of DM; and finally signal-to-noise ratio as a function of DM for each single pulse found. The bottom plot is the DM and time at which each single pulse was found. The sizes of the circles are proportional to the pulses' signal-to-noise ratios. The horizontal train of the pulses at a non-zero DM is indicative of an astrophysical source (in this case PSR B1839−04) emitting multiple pulses over the course of the observation. A modified version of the main diagnostic plot produced by `single_pulse_search.py`, including colour to represent the duration of the each single pulse (in number of samples) is also used. The pulse duration adds a useful diagnostic: a pulse detected with the optimal DM will have the largest signal-to-noise and the smallest duration. As the DM diverges from the optimal DM, the signal-to-

[1]It is mentioned in Section 2.2.3 that magnetars are not expected to be accelerated. Also, even for the most extreme parameters (e.g. a $B = 10^{16}$ G, $P = 1$ s magnetar), the drift due to the spin-down $\dot{P}$ is expected to be only ~ 1 Fourier bin over the course of a 12 hour observation. Thus, the search in $\dot{P}$ is not strictly necessary for magnetars. Nevertheless, a search is conducted to confirm this.

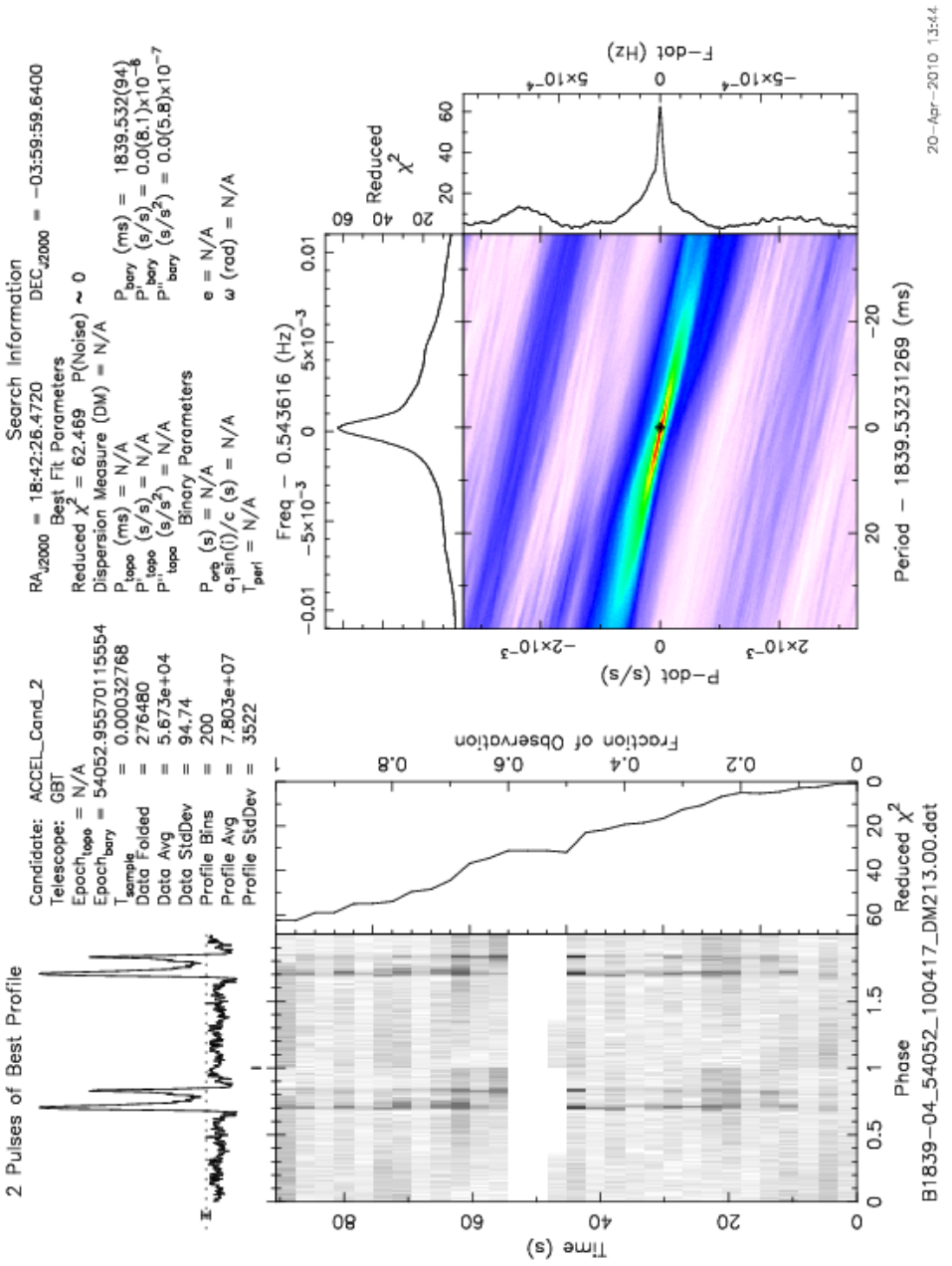

Figure 2.4: Diagnostic plot for periodicity candidates as produced by `prepfold`. The various elements of the plot are described in the text (see Section 2.3). This fold is of PSR B1839−04. The white band in the sub-integrations plot (at ~ 50 s) is due to the excision of a burst of RFI.

noise ratio of the detected pulse will drop off and the apparent duration of the pulse will increase. This is because using a non-optimal DM smears the pulse (see Section 2.2.2). An example of this type of plot is shown in Figure 2.6.

2.4 End-To-End Example: PSR B1839−04

To summarize the data path and data products, as described in Sections 2.2 and 2.3, the salient points will be presented within the context of a 90 s observation of PSR B1839−04, a 1.84 s pulsar with a DM of 196 cm^{-3} pc.

First, a RFI mask removing 11% of the observation was generated from the un-dedispersed data. This mask was used during dedispersion. In total, 504 dedispersed time series were produced between DM = 0 cm^{-3} pc and DM = 503 cm^{-3} pc. Also, during the dedispersion step, the data were barycentred and downsampled by a factor of 4, to an effective sample time of 327.68 μs. Each of these time series was searched for single pulses, period signals and folded with an ephemeris[1]. The pulsar was discovered in the periodicity search at an appropriate period and DM. It was also detected at a resonable DM when using the ephemeris to fold dedispersed time series. Finally, bright single pulses were also discovered from PSR B1839−04 centred around DM $\sim$ 200 cm^{-3} pc. Plots produced by `prepfold` and `single_pulse_search.py` were used as examples in Section 2.3.

[1]The ephemeris used was downloaded from the ATNF pulsar catalogue.

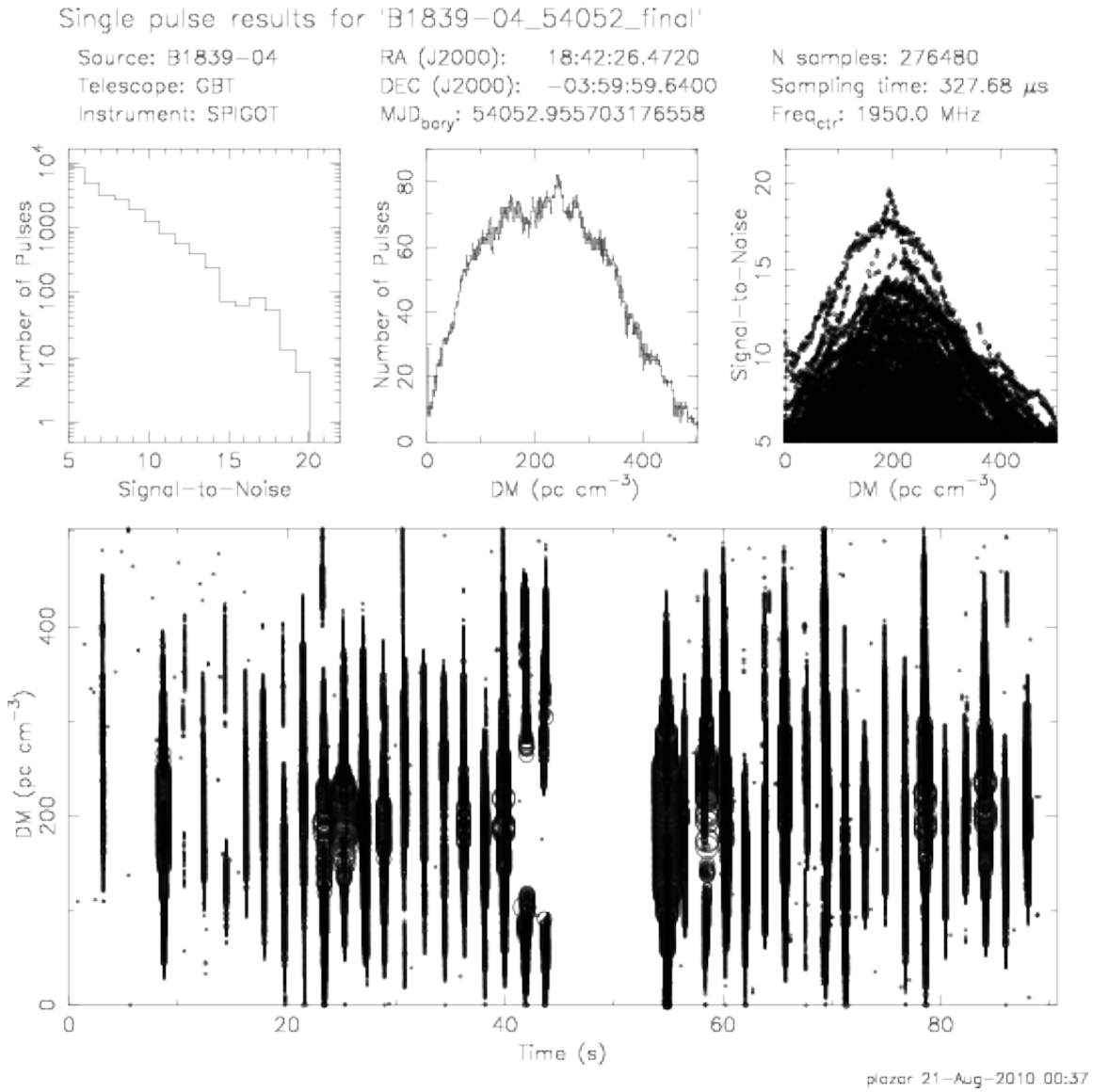

Figure 2.5: Diagnostic plot for bright single pulses, down to a signal-to-noise ratio of 5, produced by `single_pulse_search.py` for an observation of PSR B1839−04. The various elements of the plot are described in the text (see Section 2.3).

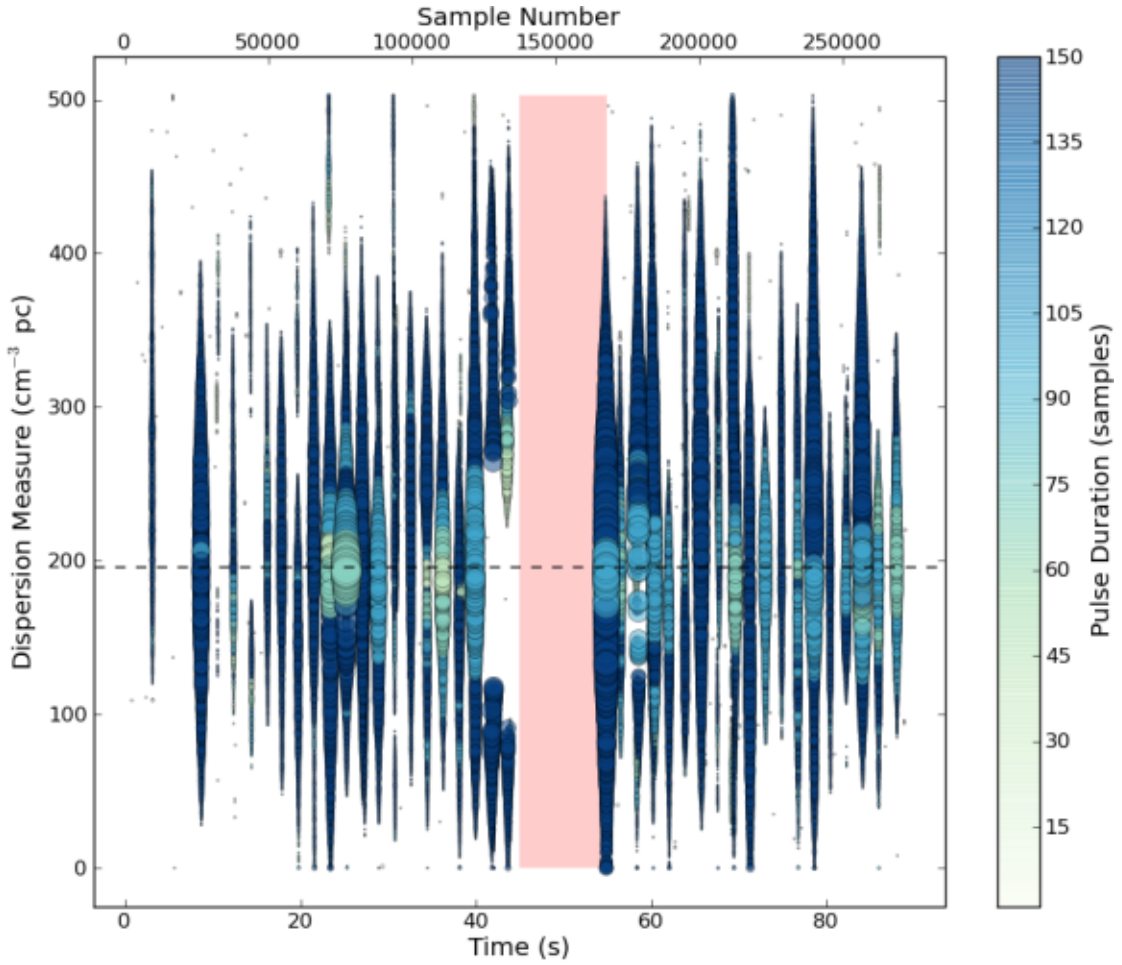

Figure 2.6: A colour plot of the single pulses detected by `single_pulse_search.py` for an observation of PSR B1839−04. Single pulses with signal-to-noise $\gtrsim 5$ are shown. The size of each circle is proportional to the signal to noise. The colour scale is related to the duration of the pulse (in number of samples). The red band is a region masked due to RFI. The horizontal dashed line indicates the DM of PSR 1839−04, 196 cm^{-3} pc, as taken from the ATNF Pulsar Catalogue. More details can be found in the text.

3
Observations

You can observe a lot by just watching.

Yogi Berra

In this chapter the details of the observing proposal, when and why it was submitted and what was requested, are discussed (Section 3.1). This is followed by an overview of the seven sources observed in the during the telescope time granted (Section 3.2). Finally, the observations analysed in this thesis are summarized (Section 3.3).

3.1 The Project and Objectives

In 2006, a proposal (ID# `GBT06C-045`) was submitted to the Green Bank Telescope (GBT) to observe seven confirmed magnetars: 1RXS J170849.0−400910, 1E 1841−045, 1E 2259+586, 4U 0142+61, SGR 1806−20, SGR 1900+14, XTE J1810−197, and two magnetar candidates: AX J1845−0258, and GRB 050925. The proposal consisted of two parts: The first part was to observe each source in an attempt to detect radio emission, or in the absence of such a detection, place an upper limit on the presence of such emission that could be used as a baseline for comparison should the source be detected at radio frequencies in the future. The second part of the proposal was a series of Target-of-Opportunity (ToO) observations that would be triggered if one of the proposed sources was seen to have an "event," as detected by X-ray monitoring. The various types of events observed in magnetars that could be used to trigger a ToO are described in Section 1.3. The ToO observations were to be scheduled at increasing intervals after the outburst, the first observation as soon as possible, then 1 day, 3 weeks, 2 months, and 8 months following the event.

The proposal was accepted and scheduled to begin in fall 2006. Two magnetars, XTE J1810−197 and 1RXS J170849.0−400910, were not observed as part of this project. The then-recently discovered transient magnetar XTE J1810−197 was dropped from the project as it was already being studied in detail in the radio regime (e.g Camilo et al., 2006, 2007c,a). The low declination of 1RXS J170849.0−400910 ($\delta \sim -40°$) made it impractical to observe with the GBT[1] (latitude $\sim +40°$).

3.2 Sources

In this section, relevant information about each of the seven sources is presented. The basic information in the following sections can be found in the McGill SGR/AXP Online Catalog and references therein.

Distance estimates can be used to estimate the DM of each source. To do this, a model of the Galactic free electron density is required. When provided with a line-of-sight and a distance, the `NE2001` model (Cordes & Lazio, 2002) can be used to compute the expected DM[2].

1E 1841−045

The AXP 1E 1841−045 has a rotational period of 11.8 s (Vasisht & Gotthelf, 1997). The estimated distance to this source is $8.5^{+1.3}_{-1}$ kpc (Tian & Leahy, 2008), which, together with the source's position, suggests a DM of ~ 800 cm^{-3} pc. The supernova remnant[3] Kes 73 is associated with 1E 1841−045.

1E 1841−045 is regularly monitored by NASA's *Rossi X-ray Timing Explorer*[4] (*RXTE*, Dib et al., 2008; Dib, 2009). The analysis of these data allow for an accurate rotational ephemeris. The ephemeris used to fold radio data of this source is shown

[1] See GBT proposer's guide: http://www.gb.nrao.edu/gbtprops/man/GBTpg.pdf

[2] As a rule-of-thumb among the radio pulsar community, the DM along any given line-of-sight returned by the model is assumed to be uncertain by up to 50%.

[3] Kes 73 is also referred to as G27.4+0.0 in Green's online Catalogue of Galactic Supernova Remnants: http://www.mrao.cam.ac.uk/surveys/snrs/.

[4] Information about *RXTE* monitoring targets and observations can be found on the telescope's website: http://heasarc.gsfc.nasa.gov/docs/xte/.

Table 3.1: Rotational ephemerides used for 1E 1841−045, 1E 2259+586, and 4U 0142+61.

Parameter	**1E 1841−045**	**1E 2259+586**	**4U 0142+61**
Right Ascension (J2000)	18:41:19.2	23:01:07.9	01:46:22.3
Declination (J2000)	−04:56:12.5	58:52:46.0	61:45:07.0
Frequency (Hz)	0.084863091(5)	0.14328613(6)	0.1150918267(8)
Frequency derivative (10^{-15} Hz/s)	−289(2)	−7(5)	−26.89(6)
Epoch (MJD)	54053	54050	53919
Reference	Dib et al. (2008)	Dib (2009)	Dib et al. (2007)

NOTES:

Uncertainties reported are the 1-σ uncertainties produced by `TEMPO`. Values without uncertainties were not fitted for in these ephemerides.

Ephemerides are update versions (provided by R. Dib, private communication) of what is reported in the references listed.

in Table 3.1.

1E 2259+586

The period of 1E 2259+586 is 6.98 s, and it is estimated to be at a distance of 4.0 ± 0.8 kpc (Fahlman & Gregory, 1981; Tian et al., 2010). This distance and the source position correspond to a line-of-sight DM of ∼150 cm^{-3} pc. 1E 2259+586 is associated with the supernova remnant[1] CTB 109.

1E 2259+586 is also regularly monitored using *RXTE* (Dib, 2009). Using these data, an ephemeris was computed. This ephemeris shown in Table 3.1 was used to fold the radio data.

4U 0142+61

4U 0142+61 has a period of 8.69 s. The distance to this source is estimated to be 3.6 ± 0.4 kpc (Durant & van Kerkwijk, 2006). This distance, in the direction of 4U 0142+62, yields a DM of ~ 100 cm^{-3} pc.

The rotational ephemeris for 4U 0142+61 used to fold the radio data of this target is shown in Table 3.1. The ephemeris was computed using *RXTE* data from regular

[1]CTB 109 is also known as G109.1-1.0 in Green's catalogue.

monitoring observations (Dib et al., 2007).

Within a few months before and after the start of the observations with the GBT, six X-ray bursts were detected from 4U 0142+61 with *RXTE* (Gavriil et al., 2007, 2009). The six bursts were detected in three separate observations on MJDs 53831 (one burst), 53911 (four bursts) and 54138 (one burst). The last of the six bursts was the brightest in terms of peak flux and occurred, fortuitously, while the `GBT06C-045` ToO proposal was still active, allowing for additional observations to be triggered. Observations of 4U 0142+61 were made on the day of the burst, as well as at intervals of 1 day, 1 week, 3 weeks, 2 months and 8 months after the burst.

AX J1845−0258

The AXP candidate AX J1845−0258 was detected in a single 1993 *Advanced Satellite for Cosmology and Astrophysics* (*ASCA*) observation with a periodicity of $P = 6.97$ s (Torii et al., 1998). The distance to the pulsar is estimated to be ~ 8 kpc (Torii et al., 1998). This distance corresponds to a DM of ~ 750 cm^{-3} pc. AX J1845−0258 is spatially coincident with the supernova remnant G29.6+0.1 (Gaensler et al., 1999), suggesting that the remnant and magnetar candidate are associated.

GRB 050925

The γ-ray burst (GRB) GRB 050925 was detected as a short burst (< 128 ms) with the *Swift* satellite's burst alert telescope (BAT) on Sept. 25, 2005[1]. GRB 050925 is considered a SGR candidate because of its soft X-ray spectrum, which is uncharacteristic of short GRBs, and its localisation in the plane of the Galaxy ($l = 72.32(3)^\circ$, $b = -0.09(3)^\circ$). The absence of additional detections in any band have left this magnetar candidate unconfirmed, without a period measurement and without a distance estimate. Nonetheless the position of GRB 050925 was observed at radio wavelengths to place limits on radio emission in case another event is detected from this location.

[1]See *Swift* GCN #4034: http://gcn.gsfc.nasa.gov/other/050925.gcn3.

SGR 1806−20

The magnetar SGR 1806−20 has a rotational period of 7.56 s (Kouveliotou et al., 1998) and is estimated to be at distance of $8.7^{+1.8}_{-1.5}$ kpc (Bibby et al., 2008), which is used to predict a DM of ~ 750 cm^{-3} pc. SGR 1806−20 was observed to have a giant flare in late 2004 (See Woods & Thompson, 2006, and references therein). Following the flare, a fading, extended, unpulsed radio nebula was observed around the source (Gaensler et al., 2005). Two days after the flare, a search for pulsed radio emission was performed at 1.4 GHz using the Parkes Radio telescope. No pulsed emission was detected down to a limit of $S_{1.4} \sim 0.2$ mJy (Gaensler et al., 2005).

SGR 1900+14

SGR 1900+14 has a periodicity of 5.17 s (Kouveliotou et al., 1999). Its distance is estimated to be 12 – 15 kpc, which yields an estimated DM of ~ 700 cm^{-3} pc, using the upper limit of the distance estimate. SGR 1900+14 was observed to have a giant flare in mid-1999. Unpulsed, fading radio emission was also observed around SGR 1900+14 following the flare (Frail et al., 1999).

The relevant properties of the sources listed above are summarized in Table 3.2.

3.3 Observations

All data analysed in this thesis were recorded using the GBT at S-band (~ 1950 MHz) using the Pulsar Spigot. The observing set-up is described in detail in Section 2.1, however the key parameters are reviewed in Table 3.3.

The relatively high observing frequency was chosen to reduce the effect of dispersion by the ISM. The dispersion relation (Equation 2.1) is proportional to f^{-2}, therefore the effect of smearing at lower observing frequencies is significantly larger than at higher frequencies. This, in conjunction with magnetars' long periods, allows for larger steps in DM than would be possible at lower frequencies. Also, the large observing bandwidth available with the GBT Spigot, 600 MHz, is relatively clear of

Table 3.2: Summary of the properties of the five magnetars and two magnetar candidates observed.

Source	Period (s)	B-field (10^{14} G)	T_{sky} [a] (K)	Distance[b] (kpc)	DM Estimate (cm^{-3} pc)	SNR Assoc.
Confirmed Magnetars						
1E 1841−045	11.7750542(1)	7.1	8.00	8.5	800	Kes 73
1E 2259+586	6.978948446(4)	0.59	4.13	4.0	150	CTB 109
4U 0142+61	8.68832973(8)	1.3	3.59	3.6	100	–
SGR 1806−20	7.55592(5)	21	9.77	8.7	750	–
SGR 1900+14	5.16891778(2)	6.4	5.52	15	700	–
Magnetar Candidates						
AX J1845−0258	6.97127(3)	–[c]	8.29	8[d]	750[d]	G29.6+0.1
GRB 050925	–[e]	–[e]	4.03	17[f]	450[f]	–

NOTES:

[a] Sky temperatures include a 2.73 K contribution from the cosmic microwave background, as well as a contribution from Galactic synchrotron radiation taken from the Haslam et al. (1982) all-sky 408 MHz map. Temperatures here are reported for 1950 MHz assuming a power-law spectrum with a synchrotron index of −2.7.

[b] The distances reported here are the values used for estimating the DM, as well as for estimating luminosity limits later in this work.

[c] Candidate detected at only one epoch. No spin-down information available to estimate B-field strength.

[d] Distance very uncertain.

[e] There is no detection of this source other than the original *Swift* BAT detection. Therefore, very little information is know about this candidate.

[f] Since no distance estimate is available, the total extent of the Galaxy in the direction of GRB 050925 is assumed.

RFI. Finally, the three radio-loud magnetars have flat, or inverted, radio spectra[1] (see Section 1.4.) This suggests that the decrease in sensitivity from observing at ~ 1950 MHz is less than for most other pulsars[2]. This enables searches for radio-loud magnetars at higher-than-usual frequencies, such as S-band.

Over the course of ~ 1 year, five magnetars and two magnetar candidates were observed at radio frequencies in an attempt to detect or constrain the presence of radio emission. Data were acquired between November 13, 2006 (MJD 54052) and October 7, 2007 (MJD 54380) as part of GBT project `GBT06C-045`. The details of the 19 observations made as part of this project are shown in Table 3.4.

Table 3.3: Basic observing parameters.

Parameter	Value
Observing centre frequency	1950 MHz
Bandwidth	600 MHz
Number of channels	768
Sample time	81.92 μs

NOTES:
More details about the observing set-up can be found in Section 2.1.

Details about how the observations were analysed and the results gleaned from them are presented in Chapter 4.

[1] At the time of the proposal the only radio-loud magnetar known was XTE J1810−197. However, it was already known to have a flat spectrum.

[2] Most radio pulsars are significantly brighter at lower frequencies than at higher frequencies since on average radio pulsars have steep spectra, $\langle\alpha\rangle = -1.8 \pm 0.2$ (Maron et al., 2000).

Table 3.4: Observations of five magnetars and two magnetar candidates made as part of the project `GBT06C-045`.

Source	Epoch (MJD)	RA (J2000)	Decl. (J2000)	Obs. length (s)
1E 1841−045	54052.96	18:41:19.368	−04:56:11.4	3600
1E 2259+586	54053.14	23:01:07.848	58:52:47.28	3600
	54059.23	23:01:08.352	58:52:45.12	10800
4U 0142+61	54053.18	01:46:21.816	61:45:06.48	2340
	54056.71	01:46:22.512	61:45:07.56	1500
	54059.35	01:46:21.512	61:45:26.28	16140
	54138.95[a]	01:46:22.416	61:45:01.88	3720
	54139.82[a]	01:46:22.248	61:45:03.96	3720
	54146.33[a]	01:46:22.464	61:45:03.24	3600
	54161.51[a]	01:46:22.344	61:45:01.44	2400
	54204.59[a]	01:46:21.888	61:45:02.88	3180
	54380.10[a]	01:46:21.984	61:45:10.44	6000
AX J1845−0258	54053.01	18:44:55.368	−02:56:56.04	3600
GRB 050925	54053.09	20:13:46.92	34:19:55.2	3600
	54056.73	20:13:47.448	34:20:05.28	2760
SGR 1806−20	54190.47	18:08:39.6	−20:24:37.08	4500
	54191.48	18:08:39.96	−20:24:37.44	3720
	54211.47	18:08:40.68	−20:24:45.0	4260
SGR 1900+14	54053.05	19:07:14.976	09:19:02.64	3600

Notes:

[a] Observation is part of ToO triggered after an X-ray burst was detected on MJD 54138 using *RXTE* (Gavriil et al., 2009).

4
Anaysis and Results

Guildenstern: [...] I feel the spell about to be broken.

(*Energizing himself somewhat.*)

(*He takes out a coin, spins it high, catches it, turns it over on to the back of his other hand, studies the coin – and tosses it to* Rosencrantz. *His energy deflates and he sits.*)

Well, it was an even chance ... if my calculations are correct.

Rosencrantz: Eighty-five in a row – beaten the record!

Rosencrantz and Guildenstern are Dead

Tom Stoppard

In this chapter, details on how the observations listed in Chapter 3 were analysed are presented, as outlined in Section 2.2. The main steps of the data analysis will be discussed in turn: excision of RFI (Section 4.1), dedispersion (Section 4.2), periodicity searching and folding (Section 4.3), and single pulse searching (Section 4.4). Section 4.5 presents the results of a collection of six ToO observations of 4U 0142+61 following an X-ray burst. The results of the data analysis are presented in Sections 4.6 and 4.7. Section 4.6 contains a summary of our derived upper limits on the radio emission of magnetars, and Section 4.7 provides the results of blind searches for other pulsars in the observations.

4.1 Radio Frequency Interference

The GBT's location inside the National Radio Quiet Zone, as well as the efforts of the Green Bank Interference Protection Group, mean that RFI conditions at the telescope

are relatively good, compared to other radio telescopes (e.g. Arecibo Observatory in Puerto Rico). Unfortunately, the contamination of data from RFI cannot be entirely eliminated. Generating and applying RFI masks, using programs such as `PRESTO`'s `rfifind` are an essential step in radio data analysis. On average, $\sim 20\%$ of each data set is masked due to RFI. Table 4.1 provides an overview of the RFI masks applied to each data set analysed in this thesis.

In order to excise RFI from the data, individual frequency channels were broken into blocks, each 5 s in duration. In the time domain, blocks were masked if the mean or standard deviation was more than 7 σ from the median of all blocks in the same time interval or frequency channel. Blocks were also masked if the maximum value in their power spectrum exceeded 3 σ, when compared to the rest of their time interval or frequency channel.

In some cases, large bursts of broadband RFI cause offsets in the mean level of Spigot data (S. Ransom, private communication). This behaviour is observed in seven of the data sets analysed here, and has also been noted in other GBT Spigot data (e.g. Kondratiev et al., 2009, at 820 MHz). An example of this behaviour is shown in Figure 4.1. Data sets exhibiting this behaviour are treated differently. If the jump in the data mean occurred near the beginning or end of an observation, only the longer portion of the observation was analysed and the rest of the observation was ignored. If the jump occurred near the middle of an observation, the observation was split and each portion was analysed independently.

4.2 Dedispersion

Data were dedispersed to remove the effect of free electrons along the line-of-sight (see Section 2.2.2). Since the DM to the pulsar is not known *a priori*, many trial DMs are used to generate dedispersed time series, which are then searched. For different ranges in DM, the dedispersion plan defines the DM spacing, ΔDM, and the effective sample time, t_{samp}, which is increased by downsampling. In this thesis, the desired time resolution is between 0.5 ms and 3 ms to maintain sensitivity to short single

Table 4.1: RFI masking details.

Source	Epoch (MJD)	Fraction of time intervals masked (%)	Fraction of bandwidth masked (%)	Fraction of data masked (%)
1E 1841−045	54052.97[a]	19.1	3.9	22.6
1E 2259+586	54053.14	4.4	1.8	6.4
	54059.23[b]	3.7	0.3	4.3
	54059.29[b]	12.7	2.0	14.9
4U 0142+61	54053.18	11.9	1.8	14.0
	54056.71[a]	35.4	1.0	36.6
	54059.38[b]	6.2	0.4	7.0
	54059.48[b]	9.2	9.4	18.6
	54138.95	6.4	7.3	14.0
	54139.82	12.1	15.5	25.8
	54146.33[a]	17.8	4.2	21.6
	54161.51	12.9	15.0	26.1
	54204.58	11.9	19.1	29.3
	54380.10	10.2	13.0	22.5
AX J1845−0258	54053.01	2.2	6.1	8.5
GRB 050925	54053.09	4.6	0.4	5.7
	54056.73	20.4	14.1	31.9
SGR 1806−20	54190.47[a]	18.5	3.1	21.6
	54191.48	22.0	3.5	25.6
	54211.48[a]	8.5	2.6	11.5
SGR 1900+14	54053.05	26.0	5.7	30.8

Notes:

[a] This observation was truncated due to significant changes in the data mean caused by RFI. Additional details are provided in the text.

[b] The observation was split into smaller portions that were searched independently due to significant changes in the data mean caused by RFI. Additional details are provided in the text.

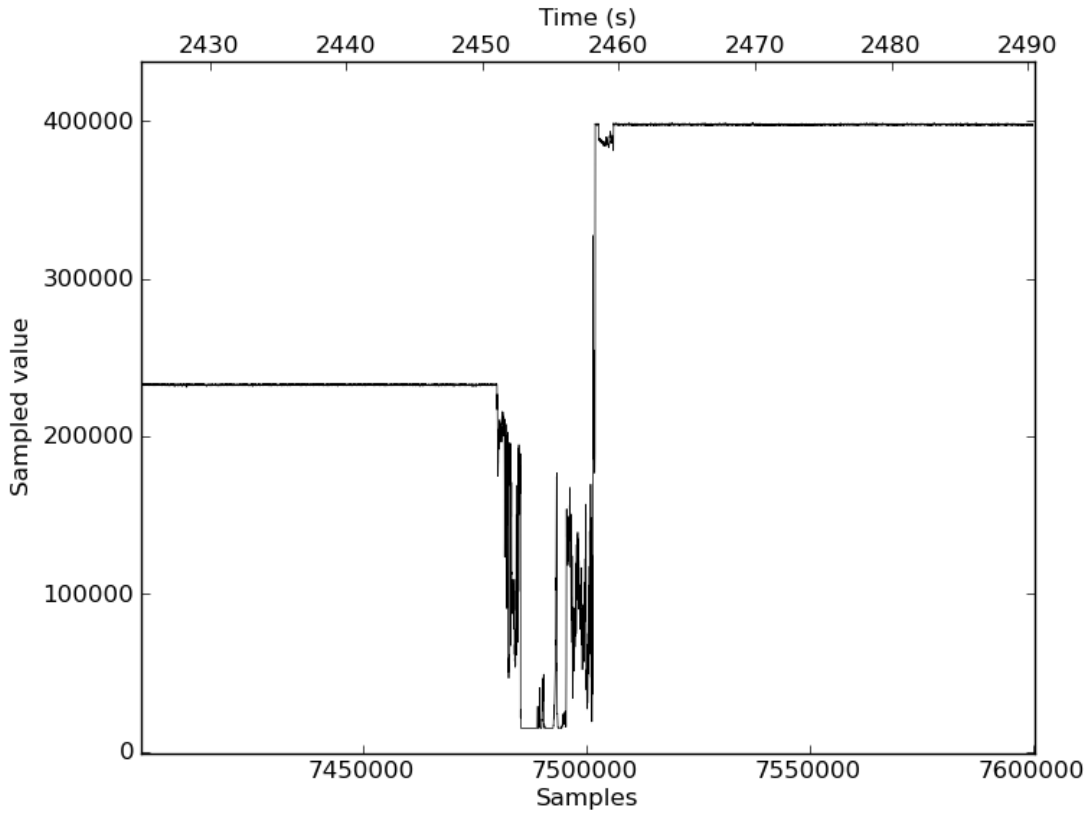

Figure 4.1: An example of a jump in mean data values caused by a large broadband burst of RFI.

pulses. The details of the dedispersion plan used is shown in Table 4.2. The method for determining this plan is described in Section 2.2.2.

The maximum DM used in searching was chosen in the following way for each source: 1) the Galactic free electron model, `NE2001` (Cordes & Lazio, 2002), was used to estimate the maximum along the line-of-sight to the source, 2) the maximum DM was chosen to be $\gtrsim 2$ times larger than the maximum DM predicted by the model. This is done to account for the possibility that there are enhancements in the DM along the line-of-sight (for example, an HII region) that are not included in the `NE2001` model. The maximum DM used for each source is shown in Table 4.3.

Table 4.2: Dedispersion plan used in this work.

DM range (cm^{-3} pc)	DM step size, ΔDM (cm^{-3} pc)	Sample time, t_{samp} (μs)
0 – 1247	1	327.68
1248 – 2446	2	655.36
$>$ 2448	3	1310.72

Table 4.3: Maximum dispersion measure used for searching, by source.

Source	DM estimate (cm^{-3} pc)	DM_{max} model[a] (cm^{-3} pc)	DM_{max} search[b] (cm^{-3} pc)
1E 1841−045	800	1650	2517
1E 2259+586	150	250	1007
4U 0142+61	100	200	503
AX J1845−0258	750	1500	2517
GRB 050925	450[c]	450	1008
SGR 1806−20	750	1650	2517
SGR 1900+14	700	800	2014

NOTES:

[a] The maximum DM predicted by the `NE2001` model along the line-of-sight.

[b] The maximum DM used for searching when generating dedispersed time series.

[c] The distance to GRB 050925 is unknown, so this DM corresponds to the maximum value possible in the Galaxy along the line-of-sight, according to the `NE2001` model.

4.3 Periodicity Search and Folding

4.3.1 Blind Periodicity Searches

Often when performing periodicity searches there is no prior knowledge of the frequency of the signal present (if any). Such a search is commonly known as a *blind* search, and requires many Fourier bins to be considered. Occasionally a signal, if present, is known to be located in a specific frequency range. This type of periodicity search can be considered an *informed* search. In this case, fewer Fourier bins need to be considered. Finally, if the exact frequency of a signal is known, the data need only be folded, not searched. Folding with a known ephemeris is described in Section 4.3.2. All data sets analysed in this thesis were searched blindly for unrelated pulsars in the beam.

In searching for periodic signals, multiple harmonics are summed to gain sensitivity to narrow peaks. The smallest duty cycle to which this technique is sensitive is inversely proportional to the number of harmonics summed, $\delta_{min} \sim 1/2N_{harm}$. To determine the number of harmonics to sum, the known radio-loud magnetars were considered. For example, XTE J1810−197 is reported to have a duty cycle of 2.7% at 1400 MHz and 1E 1547.0−5408 is observed to have a duty cycle of 14% at 2300 MHz (see Table 1.1, and references therein). The small duty cycles confirm that harmonic summing will be required to search the data analysed in this thesis optimally if all radio-loud magnetars have narrow, non-sinusoidal pulse profiles.

In this thesis, 16 harmonics were summed[1] when searching for periodic signals, providing near-optimal sensitivity for duty cycles as short as $\delta \simeq 3\%$. To ensure sensitivity to a maximal range of pulse widths, the periodicity search was also conducted with 1, 2, ..., 15 harmonics summed.

The folding parameters used for periodicity candidates identified in blind searches were determined based on the signal's period. For periods longer than 0.5 s, folding was performed with 200 bins across the pulse profile. For periods between 0.5 s and

[1]The maximum number of harmonics that can be summed using `PRESTO`'s `accelsearch` program is 16.

50 ms, 100 bins were used. For periods between 2 ms and 50 ms, 50 bins were used. Finally, for periods less than 2 ms, only 24 bins were used[1]. When folding, a small search in period and period derivative were performed around the input values.

All promising candidates (as determined by eye) identified in the output of blind periodicity searches were refolded with full frequency resolution. The frequency information allowed for an optimization of the DM of the candidate. Often, this optimization found that the best DM was in fact 0 cm^{-3} pc, which is consistent with Terrestial interference[2]. None of the magnetars or magnetar candidates, or any other new pulsars, were identified in blind searches. Details on the sensitivity of these searches are presented in Sections 4.3.3 and 4.7.

4.3.2 Folding at A Known Ephemeris

For the three magnetars with an available ephemeris, every dedispersed time series was folded using the period at the epoch of the observation. Since radio duty cycles for the magnetars searched are not known, data were folded with 16, 64, and 256 profile bins when a rotational ephemeris was available. This is done so that binning will not significantly reduce the quality of the pulse profile.

Time series for only every tenth DM-trial were examined by eye. Steps of 10 cm^{-3} pc are reasonable because the smearing across the entire 600 MHz observing band caused by an error in DM of $\delta DM = 5$ cm^{-3} pc is only 3.4 ms. For a 7 s pulsar folded with 256 bins across its profile, each bin is ~ 27 ms in duration[3]. Thus, the maximum smearing caused by an incorrect DM is unnoticeable compared to the binning used. Note that if a typical duty cycle is assumed the pulse should be wide

[1]Folding of $P < 2$ ms candidates is performed even though downsampling means there is insufficient time resolution to realistically discover extremely fast rotating pulsars. The main goal of this work is to discover slowly rotating magnetars.

[2]These RFI candiates were not originally identified at DM = 0 cm^{-3} pc because the sifting process only removes candidates with DM < 2 cm^{-3} pc. Some RFI signals are strong enough to be detected at larger DMs.

[3]The duration of each bin is even longer for longer period pulsars. The three pulsars folded with an ephemeris are 1E 1841−045 ($P \simeq 11.77$ s), 1E 2259+586 ($P \simeq 6.78$ s), and 4U 0142+61 ($P \simeq 8.69$ s).

enough that neither binning nor dispersive smearing should cause the pulse to be unresolved.

None of the observations folded with an ephemeris resulted in a detection.

4.3.3 Setting Pulsed Flux Upper Limits

As mentioned above, none of the magnetars or magnetar candidates were detected in periodicity searches. In order to place upper limits on the presence of such emission, the modified radiometer equation is used (e.g. Lorimer & Kramer, 2004),

$$S_{min} = \beta(\mathrm{S/N})_{min} \frac{\left[\left(T_{rcv} + T_{sky}\right)/G + S_{SNR}\right]}{\sqrt{n_p t_{int} \Delta f}} \sqrt{\frac{\delta}{1-\delta}}, \tag{4.1}$$

where S_{min} is the minimum detectable flux density in mJy, β is the signal degradation factor due to quantization, $(\mathrm{S/N})_{min}$ is the minimum signal-to-noise ratio considered, T_{rcv} and T_{sky} are the receiver and sky temperatures in K, respectively, G is the telescope gain in K Jy^{-1}, S_{SNR} is the flux density of the supernova remnant (if there is an association), n_p is the number of polarisations summed, t_{int} is the integration time in seconds, Δf is the observing bandwidth in MHz, and δ is the assumed duty cycle, ranging between 0 and 1.

The duty cycle is related to the width according to $\delta = W_b/P$, however this width is not the intrinsic width of the pulsar's integrated profile. The intrinsic width is effectively broadened by the finite sampling time, t_{samp}, dispersive smearing within each channel, t_{DM}, and multi-path scattering with the ISM, t_{scatt}. The broadened width is related to the intrinsic width, W_i, according to

$$W_b = \sqrt{W_i^2 + t_{samp}^2 + t_{DM}^2 + t_{scatt}^2}. \tag{4.2}$$

The scattering time, t_{scatt}, depends on the degree of inhomogeneity of the free electrons along the line-of-sight, which is predicted using the `NE2001` model for free electrons in the Galaxy (details can be found in Cordes & Lazio, 2002).

For the purposes of this work, the signal degradation factor due to quantization, β, is $\simeq 1$ since 16 bits are used to quantize the signal. The S-band receiver sys-

Table 4.4: Magnetar-supernova remnant associations and flux densities at 1950 MHz.

Magnetar	Remnant name	Flux density, S_{SNR} (Jy, at 1950 MHz)
1E 1841−045	G26.4+0.0 (Kes 73)	9.5
1E 2259+586	G109.1−1.0 (CTB109)	30.7
AX J1845−0258	G29.6+0.1	2.1

NOTES:

All flux densities are computed with values from Green's online Catalogue of Galactic Supernova Remnants (http://www.mrao.cam.ac.uk/surveys/snrs/), assuming a power-law spectral index, $S_\nu \propto \nu^\Gamma$.

tem is maintained at a temperature[1] of $T_{rcv} = 20$ K. The sky temperature, T_{sky}, is a combination of Galactic synchrotron radiation, as taken from the Haslam et al. (1982) all-sky radio map[2], and the 2.73 K contribution from the cosmic microwave background. The gain of the GBT is taken to be $G = 1.9$ K Jy^{-1}. The supernova remnant associations and their respective flux densities are shown in Table 4.4, and finally intrinsic pulse widths are taken to be between 3% and 50% of the pulse period. These widths are then broadened according to Equation 4.2.

To determine the minimum detectable signal-to-noise ratio, $(\mathrm{S/N})_{min}$, in the presence of significant RFI, a known pulsar, PSR J1907+0918, was folded using increasingly short segments of data. The resulting folds were examined by eye to determine the threshold of detectibility, $(\mathrm{S/N})_{min} = 4$. Assuming purely white noise, a 4 σ detection has a probability of $P(4\ \sigma) \simeq 3 \times 10^{-5}$ of occuring by chance.

For magnetars where a current ephemeris was available (1E 1841−045, 1E 2259+586 and 4U 0142+61), $(\mathrm{S/N})_{min} = 4$ was used since the exact period at the time of the observation was known (i.e. no searching was required).

For sources where there was an uncertainty on the folding frequency (SGR 1806−20,

[1]See the GBT proposer's guide.

[2]The electronic HEALPix version of the Haslam et al. (1982) map provided by NASA LAMBDA was used: http://lambda.gsfc.nasa.gov/product/forground/fg_haslam_get.cfm. The Galactic synchrotron emission is assumed to have a power-law spectrum with index −2.7.

SGR 1900+14, and AX J1845−0258), the value of $(S/N)_{min}$ used was in principle larger, because of the larger number of Fourier bins searched. The number of bins searched was computed by estimating the frequency at the epoch of the observation, which was extrapolated using a previously published frequency and frequency derivative, or in the case of AX J1845−0258, a previously published frequency and an assumed magnetic field strength equal to twice the largest inferred magnetic field strength for a magnetar. A conservative fractional uncertainty on the frequency of 10^{-4} was used. This was done to take into consideration the possibility of a very large glitch, or anti-glitch[1]. In all cases, the change in frequency due to a putative glitch was comparable to, or dominated, the uncertainty in the extrapolated frequency. The frequency range searched was conservatively taken to be 3 times the change in frequency due to a potential glitch or anti-glitch, as described above. This range was divided by the frequency resolution, $1/t_{int}$, to find the number of Fourier bins searched. This is equivalent to the number of independant trials. In the case of SGR 1806−20 and SGR 1900+14, the frequency range searched still only amounted to 1 Fourier bin.

The probability corresponding to 4 σ was divided by the number of Fourier bins searched and converted back to an equivalent Gaussian sigma, which was used in Equation 4.1. The estimated frequencies, frequency ranges searched and $(S/N)_{min}$ for each observation are shown in Table 4.5.

For each observation, an upper limit on the flux density of periodic emission has been computed as a function of pulse width. See Figure 4.2 for an example of dependence of the upper limit on pulse width. Assuming a duty cycle of $\delta = 5\%$, all observations have a minimum detectable flux density of $S_{min} \lesssim 0.02$ mJy or lower. By assuming a distance for each source, this can be translated to a minimum detectable luminosity of $L_{min} \lesssim 3.3$ mJy kpc^2 for all observations analysed in this thesis. The results are shown in Table 4.6.

[1] An anti-glitch is a sudden spin-down event, the opposite of a glitch, which is a sudden spin-up event.

Table 4.5: Estimated frequency for each source at each epoch, frequency range searched and the resulting minimum detectable signal-to-noise ratio.

Source	Epoch (MJD)	ν (Hz)	$\Delta\nu$ searched (Hz)	$\Delta\nu$ resolution ($\times 10^{-4}$ Hz)	N_{Trials}	$(S/N)_{min}$	Search type
1E 1841−045	54052.97	0.084863092(5)	–[a]	2.8	1	4	Ephemeris
1E 2259+586	54053.14	0.14328613(6)	–[a]	2.8	1	4	Ephemeris
	54059.23[b]	0.14328612(6)	–[a]	2.3	1	4	Ephemeris
	54059.29[b]	0.14328612(6)	–[a]	1.8	1	4	Ephemeris
4U 0142+61	54053.18	0.115091515(1)	–[a]	4.3	1	4	Ephemeris
	54056.71	0.115091507(1)	–[a]	6.7	1	4	Ephemeris
	54059.38[b]	0.115091501(1)	–[a]	1.8	1	4	Ephemeris
	54059.48[b]	0.115091500(1)	–[a]	2.5	1	4	Ephemeris
	54138.95	0.1150913157(14)	–[a]	2.7	1	4	Ephemeris
	54139.82	0.1150913136(14)	–[a]	2.7	1	4	Ephemeris
	54146.33	0.1150912985(15)	–[a]	2.8	1	4	Ephemeris
	54161.51	0.1150912633(15)	–[a]	4.2	1	4	Ephemeris
	54204.58	0.115091163(2)	–[a]	3.1	1	4	Ephemeris
	54380.10	0.115090755(3)	–[a]	1.7	1	4	Ephemeris
AX J1845−0258	54053.01	–[c]	0.116 - 0.143	2.8	100	5	Informed
GRB 050925	54053.09	–[d]	2.8×10^{-4} - 1526	2.8	5493164	6.79	Blind
	54056.73	–[d]	3.6×10^{-4} - 1526	3.6	4211426	6.75	Blind
SGR 1806−20	54190.47	0.13157(1)	0.1315 - 0.1316	2.2	1	4	Informed
	54191.48	0.13157(1)	0.1315 - 0.1316	2.7	1	4	Informed
	54211.48	0.13155(1)	0.1315 - 0.1316	2.3	1	4	Informed
SGR 1900+14	54053.05	0.1928920(6)	0.1928 - 0.1929	2.8	1	4	Informed

Notes:

[a] No frequency range searched. Ephemeris was used.

[b] The observation was split into smaller portions that were searched independently due to significant changes in the data mean caused by RFI.

[c] No frequency derivative known. Allowable range of frequencies estimated by assuming $B = 4.2 \times 10^{15}$ G.

[d] No frequency has ever been observed from this magnetar candidate.

References: *1E 1841−045*: Dib et al. (2008), *1E 2259+586*: Dib (2009), *4U 0142+61*: Dib et al. (2007), *AX J1845−0258*: Torii et al. (1998), *SGR 1806−20*: Mereghetti et al. (2005), *SGR 1900+14*: Woods et al. (2002)

Table 4.6: Upper limits on radio emission from magnetars and magnetar candidates in this thesis.

Source	Epoch (MJD)	Usable integration time (s)	Usable bandwidth (MHz)	S^{a}_{min} (mJy)	$L_{min}{}^{ab}$ (mJy kpc^2)	S_{min} single^{c} (mJy)	L_{min} single^{bc} (Jy kpc^2)	S_{min} blind^{d} (mJy)
1E 1841−045	54052.97	2395.5	576.6	0.0134	0.96	57.5	4.2	0.0226
1E 2259+586	54053.14	3439.8	589.1	0.0198	0.32	106.8	1.7	0.0336
	54059.23[e]	4238.3	598.4	0.0177	0.28	106.0	1.7	0.0302
	54059.29[e]	4953.3	588.3	0.0165	0.26	106.9	1.7	0.0283
4U 0142+61	54053.18	2060.2	589.1	0.0073	0.09	30.6	0.4	0.0123
	54056.71	825.8	593.8	0.0115	0.15	30.4	0.4	0.0191
	54059.38[e]	5256.3	597.7	0.0045	0.06	30.3	0.4	0.0078
	54059.48[e]	3564.6	543.8	0.0058	0.08	31.8	0.4	0.0099
	54138.95	3480.9	556.2	0.0058	0.08	31.4	0.4	0.0098
	54139.82	3271.3	507.0	0.0063	0.08	32.9	0.4	0.0106
	54146.33	1969.9	575.0	0.0076	0.10	30.9	0.4	0.0128
	54161.51	2089.3	510.2	0.0078	0.10	32.8	0.4	0.0131
	54204.58	2800.1	485.2	0.0069	0.09	33.7	0.4	0.0117
	54380.10	5383.9	521.9	0.0048	0.06	32.5	0.4	0.0082
AX J1845−0258	54053.01	3519.7	563.3	0.0098	0.63	40.8	2.6	0.0133
GRB 050925	54053.09	3434.9	597.7	0.0097	2.81	30.9	8.9	0.0097
	54056.73	2190.6	515.6	0.0130	3.77	33.3	9.6	0.0130
SGR 1806−20	54190.47	3520.9	581.2	0.0071	0.54	37.1	2.8	0.0121
	54191.48	2902.0	578.9	0.0078	0.59	37.2	2.8	0.0133
	54211.48	3750.7	584.4	0.0069	0.52	37.0	2.8	0.0117
SGR 1900+14	54053.05	2661.2	565.6	0.0071	1.60	38.8	7.6	0.0121

Notes:

[a] A 5% duty cycle is assumed.

[b] Distances assumed are listed in Table 3.2.

[c] Single pulse durations search are in the range 0.33 ms to 200 ms.

[d] Blind periodicity search. Assumed a 5% duty cycle, 100 ms period, and DM = 100 cm^{-3} pc.

[e] The observation was split into smaller portions that were searched independently due to significant changes in the data mean caused by RFI.

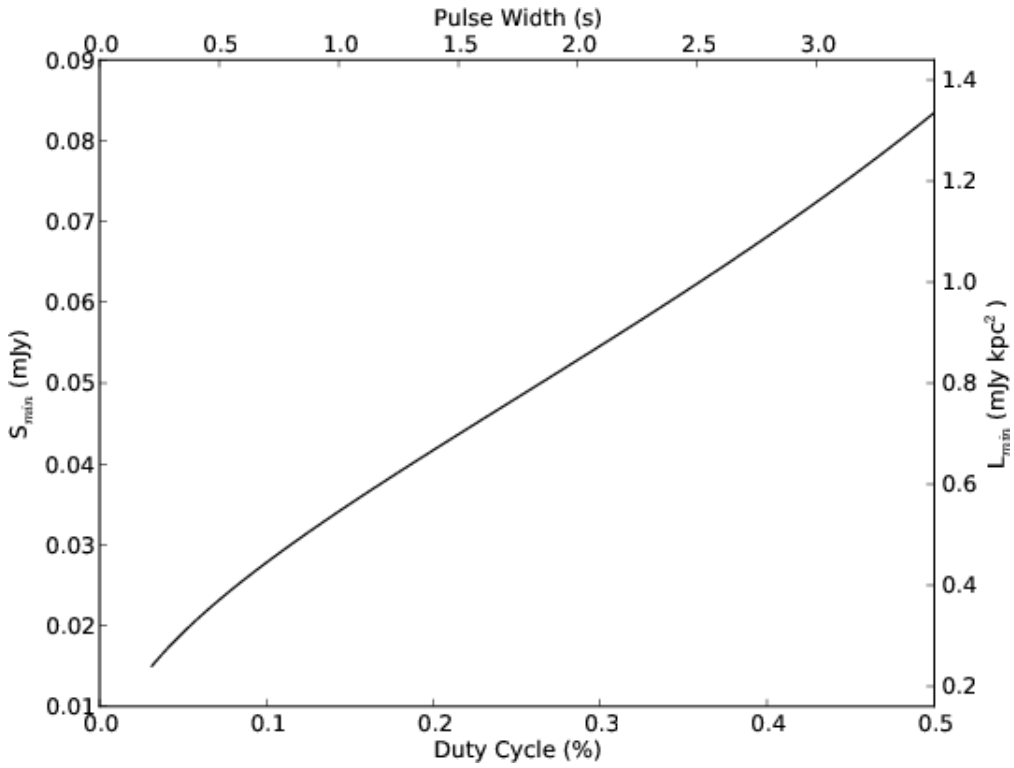

Figure 4.2: Minimum detectable luminosity limits at 1950 MHz as a function pulse width for periodic emission from 1E 2259+586 on MJD 54053. The shape of the curve on this plot is representative of similar results for other sources observed in this work.

4.4 Single Pulse Search

In addition to searching for periodic signals, the data were also searched for bright single pulses. This was done using the matched filtering technique, where time series are smoothed with top-hat filters[1] of various widths and peaks above the local mean are identified as single pulse events. The signal-to-noise ratio is highest when the top-hat width is closest to the duration of the pulse. The widths of top hats used range from 0.33 ms to 50 ms. Also, to search for longer pulses, the time series were downsampled by a factor of 4 to increase the size of each time sample. The top hats used on the downsampled time series are sensitive to pulses with durations between 1.3 ms and 200 ms.

Many single pulse events with signal-to-noise ratio > 8 were detected, however

[1]Top-hat filters are used as an estimate of the pulse profile because the actual shape of the profile is not yet known.

none were found to be consistent with an astrophysical origin. Most such events were consistent with noise, or found to be consistent with RFI, based on the lack of an appropriate frequency-dependent delay which is expected from dispersion by the ISM (see Equation 2.1).

To compute the minimum detectable flux density of single pulses in the observations, the formalism introduced in Cordes & McLaughlin (2003) was used. The relation between the brightness of a single pulse of astrophysical origin and its measured signal-to-noise ratio is given by

$$S_i = \frac{(\mathrm{S/N})_b \, S_{sys}}{W_i} \sqrt{\frac{W_b}{n_p \Delta f}}, \tag{4.3}$$

where S_i is the intrinsic flux density of the pulse, $(\mathrm{S/N})_b$ is the broadened signal-to-noise ratio, as measured by matched filtering, $S_{sys} = (T_{rcv} + T_{sky})/G + S_{SNR}$ is the system equivalent flux density, W_i and W_b are the intrinsic and broadened single pulse widths, respectively, and are related by Equation 4.2. Again, n_p is the number of polarisations summed, and Δf is the observing bandwidth. In this thesis, the minimum signal-to-noise ratio considered for a single pulse is $(\mathrm{S/N})_{b,min} = 8$. The large value of $(\mathrm{S/N})_{b,min}$ used is meant to help deal with not only noise, but also RFI. For each observation, the minimum detectable luminosity of a 10 ms single pulse for each observation is reported in Table 4.6.

The minimum detectable flux density of single pulses can be computed for the pulse durations we considered. An example of the dependence of S_{min} on pulse duration is shown in Figure 4.3.

Based on the previous discussion and the fact that no astrophysical single pulses were detected, we could conclude that the sources observed do not emit single pulses brighter than $L_{min,\ single}$, the minimum detectable single pulse luminosity. However, it is also possible the sources in question *do* occasionally emit single pulses bright enough to be detected, but the rates at which these pulses are emitted are sufficiently small that no pulses were detected in these observations. With this in mind, a 3 σ upper limit can be placed on the single pulse rate, knowing that < 1 single pulses

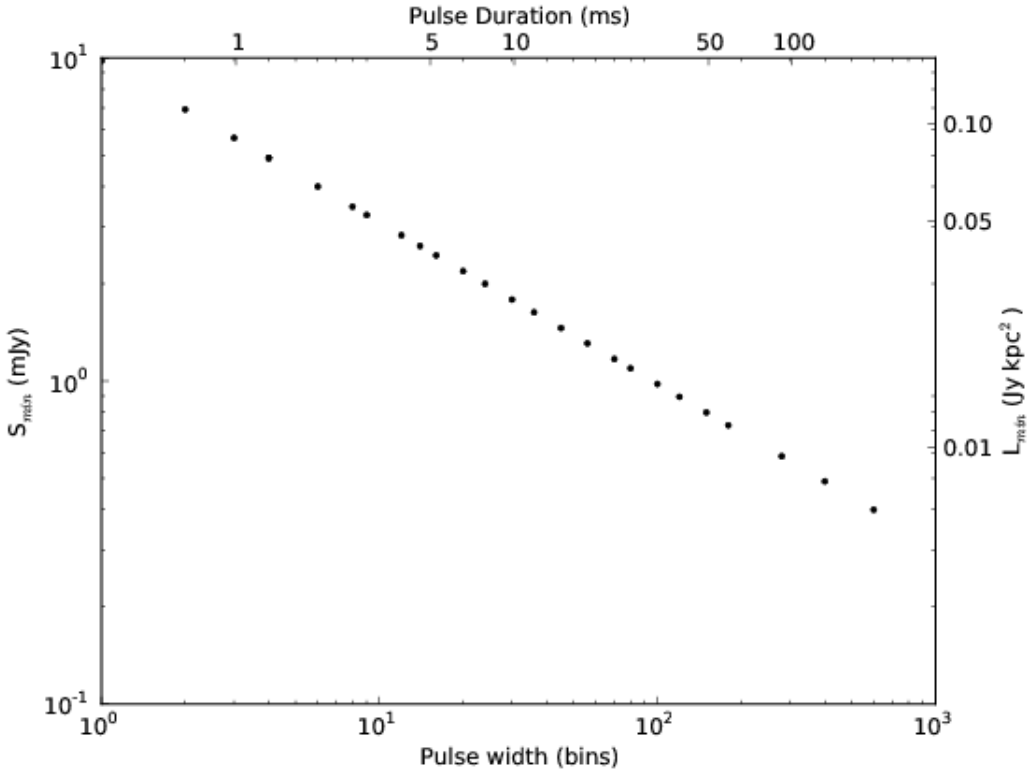

Figure 4.3: Minimum detectable flux and luminosity limits for single pulses at 1950 MHz as a function of pulse duration for 1E 2259+586 on MJD 54053. The relationship between flux or luminosity limits and pulse duration are similar for other sources studied in this work.

were detected. Because single pulses are seemingly emitted randomly, all observing time is just as likely to detect a pulse, thus we have used the sum of all unmasked integration time for each source to compute the limit on single pulse rate. The limits on single pulse rate apply only to pulses bright enough to be detected with durations between 0.33 ms and 200 ms. The computed limits on single pulse rate are shown in Table 4.7.

4.5 Target-of-Opportunity Observations of 4U 0142+61

The magnetar with the largest number of observations analysed in this thesis is 4U 0142+61, with nine observations[1]. This is thanks to a ToO proposal that was

[1]One observation was split into two parts due to RFI. Each part was analysed independently, so in total there are ten data sets from nine observations.

Table 4.7: Upper limits on single pulse rate of magnetars and magnetar candidates.

Source	Total usable time (hr)	Single pulse rate limit (hr^{-1})	Limiting L_{1950} (Jy kpc^2)
1E 1841−045	0.66	4.5	4.2
1E 2259+586	3.5	0.85	1.7
4U 0142+61	8.5	0.35	0.4
AX J1845−0258	0.98	3.1	2.6
GRB 050925	1.6	1.9	9.6
SGR 1806−20	2.8	1.1	2.8
SGR 1900+14	0.74	4.1	7.6

Notes:

The single pulse rate limit applies to pulses brighter than the limiting L_{1950} and with durations between 0.33 ms and 200 ms.

triggered after an X-ray burst was detected from 4U 0142+61 using *RXTE* on MJD 54138 (Gavriil et al., 2007, 2009). The ToO observations were deliberately spaced at increasing intervals following the burst in the hope that if radio emission following a burst has a delayed onset, as was likely the case following the X-ray outburst observed in XTE J1810−197 in 2004, it would still be detected.

In addition to the X-ray burst detected on MJD 54138, 4U 0142+61 had X-ray bursts before the start of this radio project. The other bursts were detected on MJDs 53911 and 53831. The presence of these bursts allows constraints to be placed on an even longer delayed onset of radio emission, up to $\sim$ 500 days, assuming such X-ray bursts can cause radio emission to turn on or brighten. The time scales being probed by the three burst epochs and nine observation epochs are listed in Table 4.8. The timeline of 4U 0142+61 consisting of bursts, observations analysed in this work, and a glitch that occurred on MJD 53809, is shown graphically in Figure 4.4.

None of the observations of 4U 0142+61 resulted in a detection.

Table 4.8: Time intervals between X-ray bursts from 4U 0142+61 and radio observations.

X-ray	Radio observation epochs (MJD)								
burst epochs	54053	54056	54059	54138	54139	54146	54161	54204	54380
(MJD)	*Interval between X-ray burst and radio observation epochs (days)*								
53831	222	225	228	307	308	315	330	373	549
53911	142	145	148	227	228	235	250	293	469
54138	–	–	–	0	1	8	23	66	242

4.6 Summary of Limits on Radio Emission

None of the radio observations of the magnetars and magnetar candidates outlined in Section 3.3 revealed periodic signals or bright single pulses[1]. Since no emission was detected, the observations were used to place stringent upper limits on the presence of pulsed and bursting radio emission. The results presented Sections 4.3 and 4.4 are summarized in Table 4.6.

4.7 Detecting Other Pulsars in the Field-of-View

The surface density of known pulsars on the sky is large enough to suggest that the chance inclusion of an unrelated source in an observation is possible. We therefore also searched for signals at periods far from those of the magnetar targets.

No new pulsars were discovered in any of the observations searched as part of this thesis. One previously known pulsar, PSR J1907+0918, a 226-ms pulsar with a DM of 357 cm^{-3} pc (Lorimer & Xilouris, 2000), was detected in the observation of SGR 1900+14 on MJD 54053.

The minimum detectable flux density for an unknown pulsar as a function of spin period can be computed for the blind searches performed. Representative values are computed using Equation 4.1, assuming a duty cycle of $\delta = 5\%$, a period of $P = 100$ ms and DM = 100 cm^{-3} pc. The limits of the blind searches vary between

[1]Other periodic signals and bright single pulses were detected, but they are consistent with a Terrestrial origin and are thus discarded as RFI.

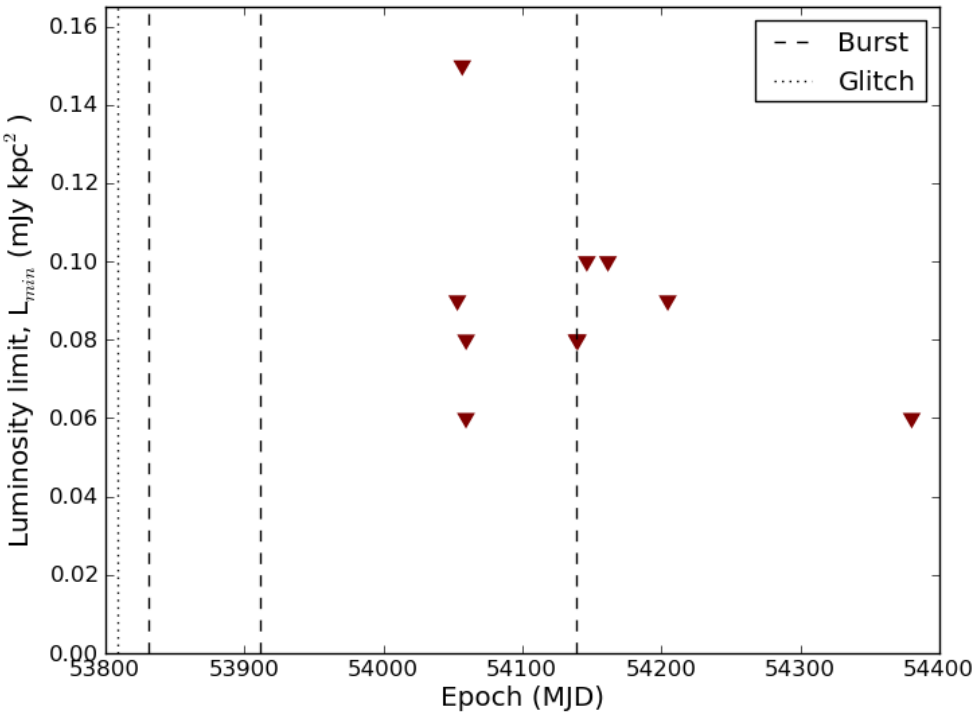

Figure 4.4: A timeline of activity for 4U 0142+61 including a glitch (dotted line), six X-ray bursts at three different epochs (dashed lines), and upper limits on radio emission at 1950 MHz (downward-pointing triangles). Note that typical luminosities for the radio-detected magnetars are significantly off the top of the plot.

observations since T_{sky} and S_{SNR} affect the system temperature. Also, the integration time and the RFI conditions (i.e. amount of data masked) are different for each observation. Typical results are reported in Table 4.6 and the dependence on DM and pulse period is shown graphically in Figure 4.5.

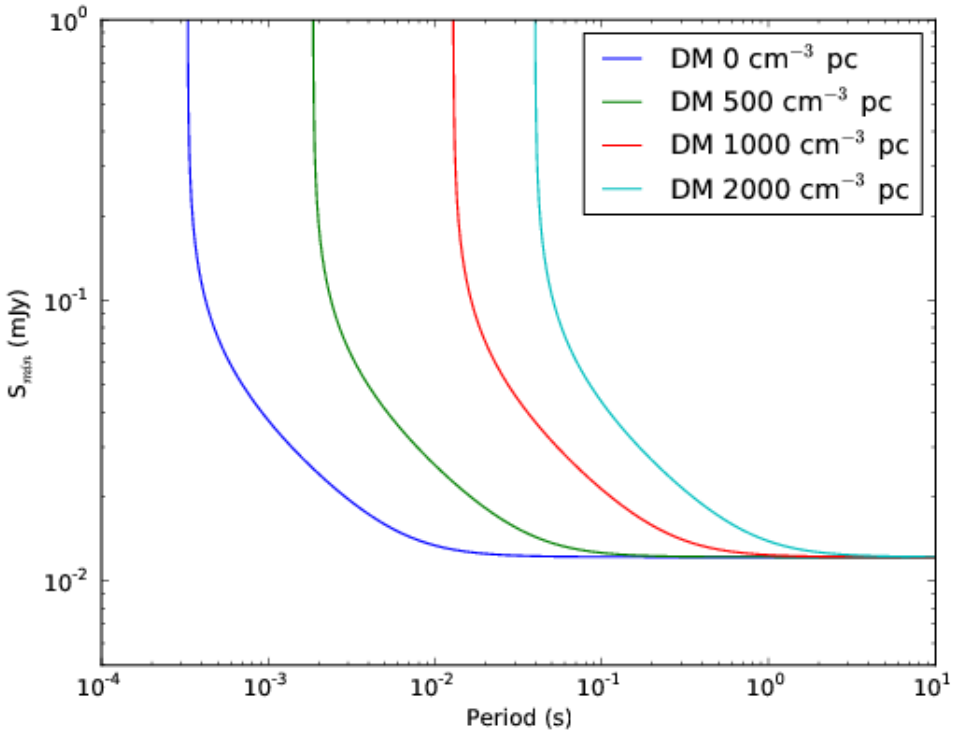

Figure 4.5: Typical flux density limits for a blind search for pulsars as a function of spin period for various DMs. These limits are for the observation of AX J1845−0258 on MJD 54053. An intrinsic duty cycle of 5% is assumed. The duty cycle is broadened by the observing system's finite sample time, dispersive smearing and scattering.

5
Discussion

What we require now is a feat of linguistic legerdemain
and a degree of intrepidity.

Spock

Star Trek VI: The Undiscovered Country

In this chapter, the upper limits on radio emission previously presented will be interpreted and put into context. This begins in Section 5.1 by comparing our results with the luminosities of radio pulsars and radio-loud magnetars, as well as comparing with the results from other radio searches for magnetars. Section 5.2 describes other effects that could cause radio emission to go undetected. Finally, Section 5.3 discusses how radio emission from magnetars is produced.

5.1 Comparision of Results

The upper limits on radio luminosities from the five magnetars and two magnetar candidates presented in Chapter 4 will now be compared to radio luminosities of a) the overall rotation-powered pulsar population, b) the three known radio-loud magnetars, and c) previous upper limits on the emission of non-radio-detected magnetars and magnetar candidates.

5.1.1 Comparison with Rotation-Powered Pulsars

There are 1402 pulsars in the ATNF database with values listed for flux density at 1400 MHz, "S1400", and spectral index, "SPINDX". For these pulsars it is possible to estimate their luminosity at 1950 MHz, L_{1950}. The median L_{1950} of the 1402 rotation-powered pulsars with luminosity measurements is 17.2 mJy kpc^2, whereas the observations analysed in this thesis result in upper limits on the magnetars'

Table 5.1: Comparison of L_{1950} of rotation-powered pulsars with magnetar upper limits from this thesis.

Source	Best L_{min} (mJy kpc^2)	Brighter pulsars (%)
1E 1841−045	0.96	94.3
1E 2259+586	0.26	98.6
4U 0142+62	0.06	99.9
AX J1845−0258	0.63	96.4
GRB 050925	2.81	84.9
SGR 1806−20	0.52	97.0
SGR 1900+14	1.60	90.3

NOTES:

Luminosities and percentage of brighter pulsars presented here do not take into consideration uncertainties in the distance of the sources.

emission at 1950 MHz that range from 60 μJy kpc^2 for 4U 0142+61 to 3.77 mJy kpc^2 for GRB 050925. Details are presented in Table 5.1. The distribution of L_{1950} for pulsars in the ATNF and the upper limits computed for the five magnetars and two magnetar candidates are shown in Figure 5.1.

We conclude that the vast majority of the known rotation-powered pulsars are sufficiently luminous to have been detected, given the sensitivity of our observations.

5.1.2 Comparison with Radio-Loud Magnetars

The three known radio-loud magnetars have properties different from those of most other radio pulsars. Most importantly, the known radio magnetars are transient, i.e. their emission is often (or possibly usually) absent. Examples of this behaviour include the sudden appearance then later fading of XTE J1810−197's radio emission over the course of $\sim$ 250 days (Camilo et al., 2007a), as well as the more sporadic behaviour observed in 1E 1547.0−5408, which, for example, was not detected in observations on January 22 and January 23, 2009, but was detected 2 days later on January 25, 2009 (Camilo et al., 2009; Burgay et al., 2009). Also, when the known radio magnetars are observed to be on, their luminosities are variable by a factor of a few (see Section 1.4

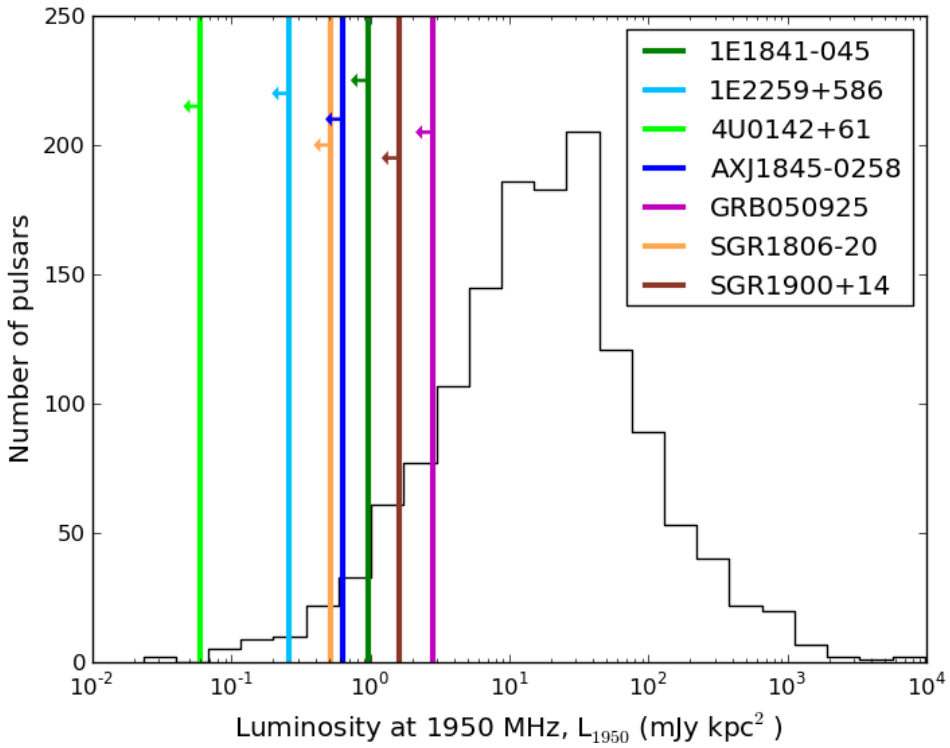

Figure 5.1: Upper limits of periodic emission from five magnetars and two magnetar candidates compared with the distribution of L_{1950} of 1402 pulsars listed in the ATNF database with "S1400" and "SPINDX" values.

for more details).

The upper limits on radio emission from magnetars derived in this thesis are significantly constraining when compared to typical luminosities observed from the three radio-loud magnetars (Table 1.1; Camilo et al., 2007a, 2008; Levin et al., 2010). However, due to the transient and variable nature of radio emission from magnetars, the results presented in this work cannot be used to provide constraints when the sources were not being observed. Thus, we cannot use the results of this work to determine if radio emission can ever be detected from our targets.

5.1.3 Comparison with Previous Limits

This work represents the first project designed to detect radio emission from a collection of magnetars and magnetar candidates at 1950 MHz. For this reason, the results presented here are not directly comparable with previously published luminosity lim-

its, which have been obtained at 430 MHz (Lorimer & Xilouris, 2000), and 1400 MHz (Burgay et al., 2006; Crawford et al., 2007; Gaensler et al., 2005). Moreover, the three known radio-loud magnetars have variable spectra with indices ranging from -1.0 to 0, in the case of XTE J1810−197 (Camilo et al., 2007c). By assuming a spectral index of -1.0, the upper limits of this work can be compared with previously published limits. In all cases, the results presented here improve upon the previous limits, ranging between a few percent better to ~ 20 times better. Thus, the results of this thesis are the most stringent constraints on the radio emission from the observed sources to date. However, as mentioned in the previous section, the complex radio behaviour exhibited by the three known radio-loud magnetars precludes this type of statement.

5.2 Other Factors Affecting Detectability

In the previous section factors intrinsic to the magnetars' emission, such as transience, variability and radio spectrum, were discussed in the context of non-detections. Other factors extrinsic to the magnetars, can also be responsible for the lack of emission observed. Two possibilities are presented below: scintillation and beaming.

5.2.1 Interstellar Scintillation

Interstellar scintillation is constructive and destructive interference caused by scattering off inhomogeneities in the ISM (e.g. Lorimer & Kramer, 2004). Scintillation has a characteristic time scale and bandwidth over which pulsar signals are enhanced or diminished. An enhanced region of flux in the time-frequency plane is called a *scintle*. The time scale and bandwidth depend on the ISM and its inhomogeneity along the line-of-sight, the distance to the pulsar, the relative transverse velocity of the pulsar with respect to the line-of-sight and the observing frequency. Intensity variations drop off for high-DM pulsars (Stinebring et al., 2000). This occurs because more scattering paths are possible. The resulting signal becomes decoherent.

For the seven sources observed as part of this thesis, the `NE2001` model was used

to estimate the scintillation bandwidth and time scales assuming the distances reported in Table 3.2 and a relative transverse velocity[1] of 100 km s^{-1}, for an observing frequency of 1950 MHz. The scintillation time scales range from 1 s to 65 s, and scintillation bandwidths range from 0.04 kHz to 120 kHz. Compared to the observing bandwidth used, $\Delta f = 600$ MHz, and the integration times, typically $t_{int} \gtrsim 30$ minutes, the scintillation scales are small. In other words, each observation averages over many scintles, thereby washing out the effect of scintillation. Therefore interstellar scintillation cannot explain why the magnetars were not detected.

5.2.2 Radio Beaming

Slowly rotating pulsars have large co-rotation radii and small polar caps, and thus are expected to have narrow radio beams (e.g. Tauris & Manchester, 1998, and references therein). Therefore, a magnetar may not be detected at radio frequencies because its radio beam does not intersect the Earth. Unfortunately, it is difficult to estimate the fraction of the celestial sphere illuminated by any given pulsar without knowing the geometry involved: the angular size of the radio beam, typically measured by its half-opening angle, ρ, and the inclination angle between the magnetic axis and the rotation axis, α. Assuming (probably naively) that the radio beaming properties of magnetars are similar to those of rotation-powered radio pulsars, empirical results for beaming fraction can be used, eliminating the need for specific knowledge of the beaming geometries. Tauris & Manchester (1998) estimate the fraction of pulsars, f, beamed towards the Earth as a function of spin period,

$$f(P) = 0.09 \left[\log \left(\frac{P}{\mathrm{s}} \right) - 1 \right]^2 + 0.03. \tag{5.1}$$

Given that there are three known radio-loud magnetars out of a total of 13 sources

[1]The 100 km s^{-1} velocity is the default used by the `NE2001` model, and cannot be changed. However, the average transverse velocities for young pulsars ($\tau_c < 3$ Myr) are ~ 300 km s^{-1} (Hobbs et al., 2005). The time scale for scintillation is inversely proportional to transverse velocity, so the larger velocities expected will cause the observation to average over even more scintles (Lorimer & Kramer, 2004).

that have been observed (this work; Burgay et al., 2006; Crawford et al., 2007; Lorimer et al., 2009) it is possible to estimate the probability that at least one of the non-detected sources is beamed towards the Earth. Using a representative period of 7 s, Equation 5.1 can be used to compute the probability that 4 or more magnetars are beamed towards the Earth (that is, at least one of the non-detected magnetars is beamed towards us) is $P(\geq 4) = 0.06\%$. This is equivalent to saying that if we had detected one of our targets, Equation 5.1 would be inconsistent with the data at the 3.2 σ level. Thus the non-detections reported here are consistent with being due to unfortunate beaming, assuming Gaussian statistics and that Equation 5.1 applies. However, three magnetars are known to be beamed towards the Earth[1] (Camilo et al., 2006, 2007b; Levin et al., 2010). The probability of three or more magnetars out of 13 being beamed towards the Earth is only $P(\geq 3) = 0.75\%$. Thus this result is inconsistent with chance at the 2.4 σ level, suggesting that Equation 5.1 does not apply to magnetar radio emission.

One possible way in which Equation 5.1 is wrong is that the Earth is not located randomly in the celestial sphere with respect to the known magnetars. That is, there could be a bias towards detecting magnetars at X-ray energies with orientations favourable for detecting radio emission. This may be the case for magnetars discovered via flares and bursts, if these phenomena are beamed tightly along the magnetic axis. However, this is unlikely be the case for magnetars discovered by their X-ray pulsations. Observed X-ray pulse profiles of magnetars are broad (e.g. Woods & Thompson, 2006), implying very broad emission regions, which likely illuminate most of the celestial sphere.

Another possibility is that the expression for beaming fraction for rotation-powered radio pulsars does not apply to magnetars. This could be due to magnetar radio beams being wider than the beams of rotation-powered pulsars with comparable periods. The relationship[2] between beam size and spin period (Tauris & Manchester, 1998),

[1]Namely XTE J1810−197, 1E 1547.0−5408, and PSR J1622−4950.

[2]This relationship is for pulsars with multiple radio components.

$$\rho\,(P) = 5.4^{\circ}\left(\frac{P}{\mathrm{s}}\right)^{-\frac{1}{2}}, \tag{5.2}$$

predicts pulsars with $P = 2$ s should have a beam size of $\rho = 2^{\circ}$, which corresponds to a duty cycle of $\delta \leq 1\%$, depending on where the line-of-sight crosses the beam[1]. This is too small to explain the observed duty cycles of the radio-loud magnetars ($\delta \sim 2.7$ to 12 %; see Table 1.1).

Another estimate can be made by assuming the sample of radio-observed magnetars (three detections out of 13 sources) is representative of the underlying population's beaming fraction. The resulting beaming fraction is $f = 23\%$. Substituting Equation 5.2 into Equation 5.1 and inverting yields an expression for ρ as a function of observed beaming fraction. Using the resulting expression, we find that $f = 23\%$ corresponds to $\rho = 9.5^{\circ}$, or in terms of duty cycle $\delta \leq 5.3\%$. Again, this result is too small to account for the duty cycles observed in radio-loud magnetars.

Finally, it is possible to estimate the size of the magnetars' radio beam by finding the value of ρ for which detecting more than 3 out of 13 sources is consistent with being due to chance at the 99.7% confidence level. The result is $\rho = 30.9^{\circ}$. This value is ~ 8 - 20 times larger than what is predicted by Equation 5.2 for rotation-powered pulsars with magnetar-like spin periods ($P \sim 2$ - 12 s). Also, the estimated beam size corresponds to duty cycles of $\delta \leq 17.3$ %, which is consistent with observations of radio-magnetar profiles.

Without a firm understanding of the radio beam sizes of radio-loud magnetars, it is difficult to determine their beaming fraction. However, the result that radio beams of 3 out of 13 magnetars are known to intersect the Earth strongly suggests that the geometrical properties of their radio emission are different from those of rotation-powered pulsars.

[1]Because ρ is the half-opening angle of the beam, the maximum duty cycle is $\delta_{max} = 2\rho/360^{\circ}$.

5.3 Consequences on the Physics of Magnetars

It is unclear exactly how radio emission in rotation-powered pulsars is produced (e.g. Lorimer & Kramer, 2004), let alone if radio emission from magnetars is produced by the same mechanism. It has been proposed that the ultra-strong, twisted magnetic field possessed by magnetars could enable types of radio emission not possible in rotation-powered pulsars (see Camilo et al., 2006, and references therein). One idea is that some of the radio emission from magnetars can be emitted along closed magnetic field lines. This could explain the origin of the wider radio beams suggested in Section 5.2.2, and account for the apparent surplus of sources beamed towards the Earth.

Phenomenologically, it is known that radio emission can turn on and off in a variety of ways, such as pulse nulling (Wang et al., 2007) and sporadic single pulses as in the so-called rotating radio transients (McLaughlin et al., 2006). Another such way is exhibited by the intermittent pulsar B1931+24 (Kramer et al., 2006). This pulsar's intermittency is quasi-periodic. Its "on" phase lasts $\sim$ 5 - 10 days and its "off" phase lasts $\sim$ 25 - 35 days. The pulsar is observed to spin down $\sim$ 50% more rapidly in its "on" phase than during its "off" phase. It has been suggested that the difference in spin-down rates is caused by an increase in torque due to higher densities of charged plasma in the magnetosphere compared to the "off" phase. The intermittent behaviour of PSR B1931+24 may have relevance to magnetars and their variable radio emission. It is conceivable that radio emission from magnetars also requires sufficient plasma densities in the emitting region. In fact, the torque variations exhibited by XTE J1810−197 as its flux decreased can be interpreted as being due to changes in the density of plasma in the magnetosphere (Camilo et al., 2007a), and is consistent with the model presented in Kramer et al. (2006).

As mentioned in Section 1.4, two of the three radio-loud magnetars, XTE J1810−197 and 1E1547.0−5408, were detected only after X-ray events (Camilo et al., 2006, 2007b). However, Levin et al. (2010) suggest that PSR J1622−4950 became bright at radio frequencies without an X-ray outburst, based on their search of archival X-ray

data[1]. It is possible that an X-ray burst was missed. Therefore, it is worthwhile to increase the total number of epochs at which each source is observed, as this will increase the chances that radio emission will be detected, since an X-ray event may not signal a radio turn-on, or X-ray events, if they are required, can be missed. Also, in the absence of a detection, establishing baselines at multiple frequencies will be useful for comparative purposes should any of the observed sources become radio bright in the future.

One thing is clear: studying the transient behaviour of radio emission from magnetars, namely the properties of the radio emission as it turns on and off, the properties of any X-ray emission that accompanies such an event, as well as the conditions under which these occur, will likely help understand how radio emission is produced, both in magnetars and rotation-powered pulsars. Therefore, continued vigilance and monitoring in the radio and X-ray regimes is warranted.

[1]Levin et al. (2010) searched data from *Chandra*, *XMM-Newton*, *Rosat*, *ASCA*, *Beppo-SAX*, *RXTE*, and *Swift* for X-ray outbursts or flux enhancements. None were found.

6
Conclusion

If you've heard this story before, don't stop me, because
I'd like to hear it again.

Groucho Marx

The ultimate goal of this work was to increase the number of magnetars known to emit at radio frequencies. To this end, 19 observations of five magnetars and two magnetar candidates were made using the GBT using the Spigot at 1950 MHz. The data were searched for pulsed periodic emission, as well as bright single pulses using the methods described in Chapter 2.

Unfortunately, none of the sources observed were detected. The non-detections were used to place stringent constraints on the presence of such radio emission in the data. None of the seven sources observed are brighter than 3.77 mJy kpc^2 in any of the data sets. Details of the upper limits on radio emission were presented in Chapter 4.

It is difficult to use the upper limits derived from this work to constrain the physical properties of the sources, since previous results suggest radio emission from magnetars is highly variable. It is possible that observations were merely scheduled, by chance, at times when the magetars' radio emission was too faint to be detected. On the other hand, it is also possible that the non-detections are nothing more than unfortunate beaming geometries. However, this work and previous work have combined to detect three out of 13 magnetars observed at radio frequencies. This suggests that the radio beaming fraction of magnetars is larger than that of rotation-powered pulsars with similar periods.

Looking forward, if any of the sources studied here becomes visible at radio frequencies in the future, the results reported here will be invaluable for providing a

baseline with which detections can be compared. This will possibly help us understand what magnetospheric conditions are required to produce radio emission, such as the nature of the magnetic fields of magnetars, and the details of plasmas and currents in magnetar magnetospheres. What is learned about magnetars could also likely help elucidate the radio emission mechanism for pulsars in general. For this reason, the known magnetars should continue to be observed at radio frequencies in the hopes of a turn-on. Current and future telescopes capable of forming multiple independent beams on the sky, such as the *Low Frequency Array* (*LOFAR*) and the *Square Kilometer Array* (*SKA*)[1], will enable astronomers to detect the turn-on of radio emission from magnetars in near real-time and allow their variability to be tracked more closely.

The key in the progression of knowledge outlined above is to continue studying the known magnetars at radio frequencies and other wavebands. Also, it is important to continue searching for new magnetars, and to continue searching for radio emission from known magnetars at different epochs and frequencies using ever-more sensitive telescopes, instruments and techniques, as this work has done.

[1] *LOFAR*: http://www.lofar.org/, and the *SKA*: http://www.skatelescope.org/.

Bibliography

Abdo, A. A. et al. 2010, ApJ Supp., 187, 460

Archibald, A. M., Kaspi, V. M., Livingstone, M. A., & McLaughlin, M. A. 2008, ApJ, 688, 550

Baring, M. G. & Harding, A. K. 1998, ApJL, 507, L55

Bibby, J. L., Crowther, P. A., Furness, J. P., & Clark, J. S. 2008, MNRAS, 386, L23

Bracewell, R. N. 2000, *The Fourier Transform and its Applications*, 3rd ed. (McGraw-Hill)

Burgay, M., Israel, G. L., Possenti, A., Rea, N., Esposito, P., Mereghetti, S., Tiengo, A., & Gotz, D. 2009, The Astronomer's Telegram, 1913, 1

Burgay, M., Rea, N., Israel, G. L., Possenti, A., Burderi, L., di Salvo, T., D'Amico, N., & Stella, L. 2006, MNRAS, 372, 410

Camilo, F., Cognard, I., Ransom, S. M., Halpern, J. P., Reynolds, J., Zimmerman, N., Gotthelf, E. V., Helfand, D. J., Demorest, P., Theureau, G., & Backer, D. C. 2007a, ApJ, 663, 497

Camilo, F., Halpern, J. P., & Ransom, S. M. 2009, The Astronomer's Telegram, 1907, 1

Camilo, F., Kaspi, V. M., Lyne, A. G., Manchester, R. N., Bell, J. F., D'Amico, N., McKay, N. P. F., & Crawford, F. 2000, ApJ, 541, 367

Camilo, F., Ransom, S. M., Halpern, J. P., & Reynolds, J. 2007b, ApJL, 666, L93

Camilo, F., Ransom, S. M., Halpern, J. P., Reynolds, J., Helfand, D. J., Zimmerman, N., & Sarkissian, J. 2006, Nat., 442, 892

Camilo, F., Ransom, S. M., Peñalver, J., Karastergiou, A., van Kerkwijk, M. H., Durant, M., Halpern, J. P., Reynolds, J., Thum, C., Helfand, D. J., Zimmerman, N., & Cognard, I. 2007c, ApJ, 669, 561

Camilo, F., Reynolds, J., Johnston, S., Halpern, J. P., & Ransom, S. M. 2008, ApJ, 679, 681

Carroll, B. W. & Ostlie, D. A. 2006, *An Introduction to Modern Astrophysics and Cosmology*, 2nd ed. (Addison-Wesley)

Cordes, J. M. & Lazio, T. J. W. 2002, arXiv:astro-ph/0207156v3

Cordes, J. M. & McLaughlin, M. A. 2003, ApJ, 596, 1142

Crawford, F., Hessels, J. W. T., & Kaspi, V. M. 2007, ApJ, 662, 1183

Dib, R. 2009, PhD thesis, McGill University (Canada)

Dib, R., Kaspi, V. M., & Gavriil, F. P. 2007, ApJ, 666, 1152

—. 2008, ApJ, 673, 1044

Duncan, R. C. & Thompson, C. 1992, ApJL, 392, L9

Durant, M. & van Kerkwijk, M. H. 2006, ApJ, 650, 1070

Fahlman, G. G. & Gregory, P. C. 1981, Nat., 293, 202

Frail, D. A., Kulkarni, S. R., & Bloom, J. S. 1999, Nat., 398, 127

Gaensler, B. M., Gotthelf, E. V., & Vasisht, G. 1999, ApJL, 526, L37

Gaensler, B. M., Kouveliotou, C., Gelfand, J. D., Taylor, G. B., Eichler, D., Wijers, R. A. M. J., Granot, J., Ramirez-Ruiz, E., Lyubarsky, Y. E., Hunstead, R. W., Campbell-Wilson, D., van der Horst, A. J., McLaughlin, M. A., Fender, R. P.,

Garrett, M. A., Newton-McGee, K. J., Palmer, D. M., Gehrels, N., & Woods, P. M. 2005, Nat., 434, 1104

Gavriil, F. P., Dib, R., & Kaspi, V. M. 2009, arXiv:0905.1256v1

Gavriil, F. P., Dib, R., Kaspi, V. M., & Woods, P. M. 2007, The Astronomer's Telegram, 993, 1

Gavriil, F. P., Gonzalez, M. E., Gotthelf, E. V., Kaspi, V. M., Livingstone, M. A., & Woods, P. M. 2008, Science, 319, 1802

Gelfand, J. D. & Gaensler, B. M. 2007, ApJ, 667, 1111

Ghosh, P. 2007, *Rotation and Accretion Powered Pulsars* (World Scientific Publishing Co)

Gotthelf, E. V., Vasisht, G., Boylan-Kolchin, M., & Torii, K. 2000, ApJL, 542, L37

Griffiths, D. J. 1999, *Introduction to Electrodynamics*, 3rd ed. (Pretince Hall)

Halpern, J. P., Gotthelf, E. V., Becker, R. H., Helfand, D. J., & White, R. L. 2005, ApJL, 632, L29

Halpern, J. P., Gotthelf, E. V., Reynolds, J., Ransom, S. M., & Camilo, F. 2008, ApJ, 676, 1178

Haslam, C. G. T., Salter, C. J., Stoffel, H., & Wilson, W. E. 1982, A&A Supp., 47, 1

Hobbs, G., Lorimer, D. R., Lyne, A. G., & Kramer, M. 2005, MNRAS, 360, 974

Ibrahim, A. I., Markwardt, C. B., Swank, J. H., Ransom, S., Roberts, M., Kaspi, V., Woods, P. M., Safi-Harb, S., Balman, S., Parke, W. C., Kouveliotou, C., Hurley, K., & Cline, T. 2004, ApJL, 609, L21

Kaplan, D. L., Escoffier, R. P., Lacasse, R. J., O'Neil, K., Ford, J. M., Ransom, S. M., Anderson, S. B., Cordes, J. M., Lazio, T. J. W., & Kulkarni, S. R. 2005, PASP, 117, 643

Kaspi, V. M. 2007, A&Sp.Sc., 308, 1

Kaspi, V. M., Roberts, M. S. E., & Harding, A. K. 2006, Isolated Neutron Stars, eds. Lewin, W. H. G. & van der Klis, M., 279–339

Kondratiev, V. I., McLaughlin, M. A., Lorimer, D. R., Burgay, M., Possenti, A., Turolla, R., Popov, S. B., & Zane, S. 2009, ApJ, 702, 692

Kouveliotou, C., Dieters, S., Strohmayer, T., van Paradijs, J., Fishman, G. J., Meegan, C. A., Hurley, K., Kommers, J., Smith, I., Frail, D., & Murakami, T. 1998, Nat., 393, 235

Kouveliotou, C., Strohmayer, T., Hurley, K., van Paradijs, J., Finger, M. H., Dieters, S., Woods, P., Thompson, C., & Duncan, R. C. 1999, ApJL, 510, L115

Kramer, M., Lyne, A. G., O'Brien, J. T., Jordan, C. A., & Lorimer, D. R. 2006, Science, 312, 549

Kumar, H. S. & Safi-Harb, S. 2008, ApJL, 678, L43

Leahy, D. A. & Tian, W. W. 2008, A&A, 480, L25

Levin, L., Bailes, M., Bates, S., Bhat, N. D. R., Burgay, M., Burke-Spolaor, S., D'Amico, N., Johnston, S., Keith, M., Kramer, M., Milia, S., Possenti, A., Rea, N., Stappers, B., & van Straten, W. 2010, arXiv:1007.1052v1

Livingstone, M. A., Kaspi, V. M., Gotthelf, E. V., & Kuiper, L. 2006, ApJ, 647, 1286

Lorimer, D. R., Edel, S., Kondratiev, V. I., McLaughlin, M. A., Boyles, J. R., Ludovici, D. A., & Ridley, J. P. 2009, The Astronomer's Telegram, 2096, 1

Lorimer, D. R. & Kramer, M. 2004, *Handbook of Pulsar Astronomy* (Cambridge University Press)

Lorimer, D. R. & Xilouris, K. M. 2000, ApJ, 545, 385

Lyne, A. G. & Smith, F. G. 2005, *Pulsar Astronomy*, 3rd ed. (Cambridge University Press)

Malofeev, V. M., Malov, O. I., Teplykh, D. A., Tyul'Bashev, S. A., & Tyul'Basheva, G. E. 2005, Astronomy Reports, 49, 242

Manchester, R. N., Hobbs, G. B., Teoh, A., & Hobbs, M. 2005, AJ, 129, 1993

Maron, O., Kijak, J., Kramer, M., & Wielebinski, R. 2000, A&A Supp., 147, 195

McLaughlin, M. A., Lyne, A. G., Lorimer, D. R., Kramer, M., Faulkner, A. J., Manchester, R. N., Cordes, J. M., Camilo, F., Possenti, A., Stairs, I. H., Hobbs, G., D'Amico, N., Burgay, M., & O'Brien, J. T. 2006, Nat., 439, 817

McLaughlin, M. A., Stairs, I. H., Kaspi, V. M., Lorimer, D. R., Kramer, M., Lyne, A. G., Manchester, R. N., Camilo, F., Hobbs, G., Possenti, A., D'Amico, N., & Faulkner, A. J. 2003, ApJL, 591, L135

Mereghetti, S., Tiengo, A., Esposito, P., Götz, D., Stella, L., Israel, G. L., Rea, N., Feroci, M., Turolla, R., & Zane, S. 2005, ApJ, 628, 938

Ng, C., Kaspi, V. M., Dib, R., Olausen, S. A., Scholz, P., Guver, T., Ozel, F., Gavriil, F. P., & Woods, P. M. 2010, arXiv:1008.1165v1

Ng, C., Slane, P. O., Gaensler, B. M., & Hughes, J. P. 2008, ApJ, 686, 508

Ransom, S. M. 2001, PhD thesis, Harvard University (U.S.A.)

Ransom, S. M., Eikenberry, S. S., & Middleditch, J. 2002, AJ, 124, 1788

Shearer, A. & Golden, A. 2002, in Neutron Stars, Pulsars, and Supernova Remnants, eds. W. Becker, H. Lesch, & J. Trümper, 44–+

Shitov, Y. P., Pugachev, V. D., & Kutuzov, S. M. 2000, in Astronomical Society of the Pacific Conference Series, Vol. 202, IAU Colloq. 177: Pulsar Astronomy - 2000 and Beyond, eds. M. Kramer, N. Wex, & R. Wielebinski, 685–+

Stinebring, D. R., Smirnova, T. V., Hankins, T. H., Hovis, J. S., Kaspi, V. M., Kempner, J. C., Myers, E., & Nice, D. J. 2000, ApJ, 539, 300

Tauris, T. M. & Manchester, R. N. 1998, MNRAS, 298, 625

Tian, W. W. & Leahy, D. A. 2008, ApJ, 677, 292

Tian, W. W., Leahy, D. A., & Li, D. 2010, MNRAS, 404, L1

Torii, K., Kinugasa, K., Katayama, K., Tsunemi, H., & Yamauchi, S. 1998, ApJ, 503, 843

Vasisht, G. & Gotthelf, E. V. 1997, ApJL, 486, L129+

Wang, N., Manchester, R. N., & Johnston, S. 2007, MNRAS, 377, 1383

Wilson, T. L., Rohlfs, K., & Hüttemeister, S. 2009, *Tools of Radio Astronomy*, 5th ed. (Springer-Verlag)

Woods, P. M., Kouveliotou, C., Göğüş, E., Finger, M. H., Swank, J., Markwardt, C. B., Hurley, K., & van der Klis, M. 2002, ApJ, 576, 381

Woods, P. M. & Thompson, C. 2006, Soft Gamma Repeaters and Anomalous X-ray Pulsars: Magnetar Candidates, eds. Lewin, W. H. G. & van der Klis, M., 547–586